EFFECT OF THE POSITION OF THE DOUBLE-BOND IN MONOUNSATURATED PHOSPHOLIPIDS ON THE DYNAMICS OF MODEL MEMBRANES

By

Tatiana Zaraiskaya

A THESIS SUBMITTED IN PARTIAL FULFILLMENT OF

THE REQUIREMENTS FOR THE DEGREE OF

MASTER OF SCIENCE

in

THE FACULTY OF MATHEMATICS AND SCIENCE

DEPARTMENT OF PHYSICS

BROCK UNIVERSITY

April 1999

Abstract

Thermodynamics of model membrane systems containing monounsaturated phospholipids is strongly influenced by the position of the C=C double bond in the acyl chain. The temperatures of both chain-melting (T_M) and $L_\alpha \rightarrow H_{II}$ (T_H) phase transitions are lowered by up to 20°C when C=C is moved from positions 6 or 11 to position 9 in an 18-carbon chain. This work is an attempt to elucidate the underlying molecular mechanisms responsible for these dramatic thermodynamic changes.

Mixtures of di-18:1 phosphatidylethanolamine with C=C at positions 6, 9, 11 were used, with a small amount of perdeuterated tetradecanol, known to be a good reporter of the chain molecular order. Spectral second moments were used to monitor the $L_\alpha \rightarrow H_{II}$ phase transition, which was found to be broad (2—6°C), with a slight hysteresis on heating/cooling. The orientational order profiles were measured using ^{2}H nuclear magnetic resonance and changes in these order profiles between L_α and H_{II} phases show both a local increase in order in the vicinity of the C=C bonds and an overall decrease in the average orientational order of the chain as a whole. These subtle changes require both high-fidelity spectroscopy and a careful data analysis that takes into account the effects due to partial magnetically-induced orientational ordering of the bilayers. In the context of some recently reported cross-relaxation measurements in similar phospholipids, our results suggest that large-amplitude conformational changes in the interior of the model membranes play a more significant role than previously thought.

Table of Contents

List of Figures

Acknowledgement

I thank my supervisor Professor Ed Sternin for his guidance, encouragement, understanding and financial support over these two years. I also would like to thank Professor Richard Epand for his help in sample preparation and discussions of the results obtained.

I am grateful to all faculty of Physics Department for providing a nice working atmosphere. My special thanks to Frank Benko.

Finally, I want to thank Mrs.Hallett for her encouragement and support in my first steps on the Land of Maple Leaf.

Introduction

The problem treated in this thesis was stimulated by the recently established fact that the introduction of unsaturation into the acyl chain reduces drastically the transition temperature of the lipids [16]. A minimum in the temperature of the lamellar-to-hexagonal ($L_\alpha \rightarrow H_{II}$) phase transition ($T_H$) was observed when the double bond was around position 9 in an 18-carbon chain. Similar results have been found for the chain-melting phase transition (T_M) in other lipids [3]. However, the mechanism responsible for these thermodynamic changes is still unknown.

The present work is an attempt to understand the possible molecular mechanism that might be responsible for this behavior. Mixtures of phosphatidylethanolamine (PE) lipids with double bonds (C=C) at carbon position 6, 9, 11 ($\triangle 6$, $\triangle 9$, $\triangle 11$), as counted from the polar head, were used with small amount of perdeuterated tetradecanol (TD). In this work TD was used to report about the chain molecular order of the host lipid [27, 49]. It is well established that the presence of TD shifts the $L_\alpha \rightarrow H_{II}$ phase transition compared to the case of pure lipids, but does not modify the order of the lipid chains [27].

The orientational order profiles were measured using deuterium magnetic resonance (^{2}H NMR) in the L_α and H_{II} phases. Changes in the order profiles between L_α and H_{II} phases are shown to be sensitive to the location of the C=C bonds.

Spectral second moments were used to monitor the phase transition. The analysis indicates that mixtures of di-18:1 PE lipids and TD undergo a broad phase transition accompanied by a slight hysteresis on heating/cooling.

In Chapter 1 I provide some background knowledge of plasma membranes and lipid

bilayers, as well as a description of some of their thermodynamic properties. Chapter 2 presents a brief review of elementary NMR theory in the classical and the quantum mechanical pictures. Chapter 3 introduces the 'order parameter' and describes the distribution of domain orientations present in the sample. Chapter 4 includes the procedure used in sample preparation and the details of the experiments performed as well as methods used to obtain the orientational order parameters from spectroscopic data. In Chapter 5 the results and a discussion are presented. At the end of the thesis concluding remarks are given.

Chapter 1

Membranes

A plasma membrane encloses every cell, defining the cell's extent and maintaining the essential differences between its contents and the environment. This membrane is a highly selective filter and a device for active transport; it controls the entry of nutrients and the exit of waste products, and it generates differences in ion concentrations between the interior and exterior of the cell. The plasma membrane also acts as a sensor of external signals, allowing the cell to change in response to environmental cues. Even though each membrane exhibits unique functions, there are six features of cell membranes that are repeatedly used by a variety of membrane systems in cellular biology [32].

One motif is the transmembrane gradient of the chemical species or charge. The cell utilizes a membrane to create, maintain, or use the energy stored in a concentration gradient from one side of the membrane to the other. Examples include ions and metabolites.

A second motif is the organization of enzymes into a complex. For example, in the inner mitochondrial membrane the enzymes involved in the electron transport chain are organized into functional groups.

A third motif is control of enzyme activity by membrane structure and by individual membrane components. The interactions between membrane proteins and the lipids of the cell membrane are multifaceted and offer many possible elements of control not available to non-membrane enzymes.

A fourth motif is the membrane as substrate.

A fifth motif is the transduction of molecular information from one side of a membrane to another. For example, plasma membrane receptors function on the cell surface to recognize extracellular signals and to alter intracellular behavior in response.

A sixth motif is compartmentalization: the physical separation of one compartment from another, with control over communication between them.

The plasma membrane of the cell defines the cell boundary. This membrane by weight is about half lipid and half protein. The plasma membrane of a cell exemplifies the basic compartmental function of membranes; it separates intracellular from extracellular domains.

1.1 The Plasma Membrane and Lipid Bilayer

All biological membranes, including the plasma membrane and the internal membranes of eucaryotic cells, have a common structure: they are assemblies of lipid and protein molecules. A graphic representation of model membrane is depicted in Figure 1.1.

The lipid molecules are arranged as a continuous double layer about 5 nm thick, as shown in Figure 1.2. Polar lipids are composed of a hydrophilic polar head group and a hydrophobic chains. When lipids are set in contact with polar solvent like water the hydrophobic chains tend to cluster together in order to reduce the energy of the system (see Fig. 1.2). The *lipid bilayer* provides the basic structure of the membrane and serves as a relatively impermeable barrier to the passage of most water-soluble molecules. The protein molecules, usually 'dissolved' in the lipid bilayer, mediate many of the other functions of the membrane.

The problem of understanding the dynamics of biological membranes can be simplified if one studies model membrane systems. These systems may be entirely composed of pure phospholipid bilayers and water. The idea is that the model membranes have the same

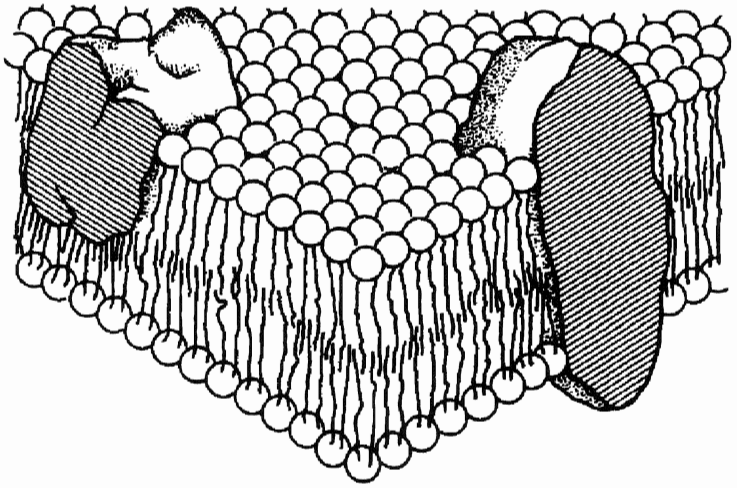

Figure 1.1: Representation of the membrane model proposed by Singer and Nicolson [42]. The large solid objects represent membrane proteins incorporated in the membrane. Reproduced from [55].

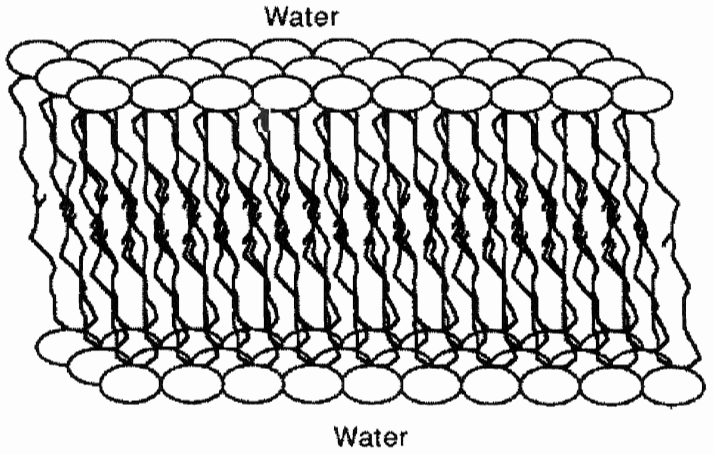

Figure 1.2: Representation of a lipid bilayer. The circles represent the lipid polar headgroups, and the wiggly lines represent the hydrophobic chains of the lipids. Reproduced from [55].

basic structure and dynamics as biological membranes [10], while their thermodynamic behavior and physical properties are considerably simpler to measure and interpret.

1.2 Motions

A cell membrane is not a rigid structure but a very dynamic body. The time scale of the motions in the bilayer range from sub-picoseconds (trans-gauche isomerization,C-C bond vibrations) to seconds (lateral diffusion). Fast motions in biomembranes exhibit axial symmetry about a long axis which is roughly perpendicular to the plane of the bilayer surface. This long axis is commonly called the director. In addition, individual lipids are free to move about the surface of the membrane. Lateral diffusion and collective undulations of the bilayer are examples of slow motion. A schematic representation of different types of motions in a bilayer is depicted in Fig. 1.3.

To define what "fast" means as applied to the molecular motions in biomembranes, one needs to consider the NMR spectroscopic time scale (τ_{NMR}). For ^{1}H and ^{2}H NMR ranges from 10^{-6}-10^{-4}s (see Table 3.1). The τ_{NMR} scale is related to the observed broadening of spectral lines. If the distribution of spectral frequencies is characterized by its second moment M_2, then the τ_{NMR} scale is given by $\tau_{NMR} = (M_2)^{(-1/2)}$.

A number of different techniques can be used to study the dynamics of phospholipids. Table 1.1 summarizes the time scales of various molecular motions and of several spectroscopic techniques that can be used to observe the effects of such motions.

1.3 Phase Transitions

Even simple two-component (lipid-water) model membrane systems can exhibit complex thermodynamic behavior. There are two types of phase transitions observed in model

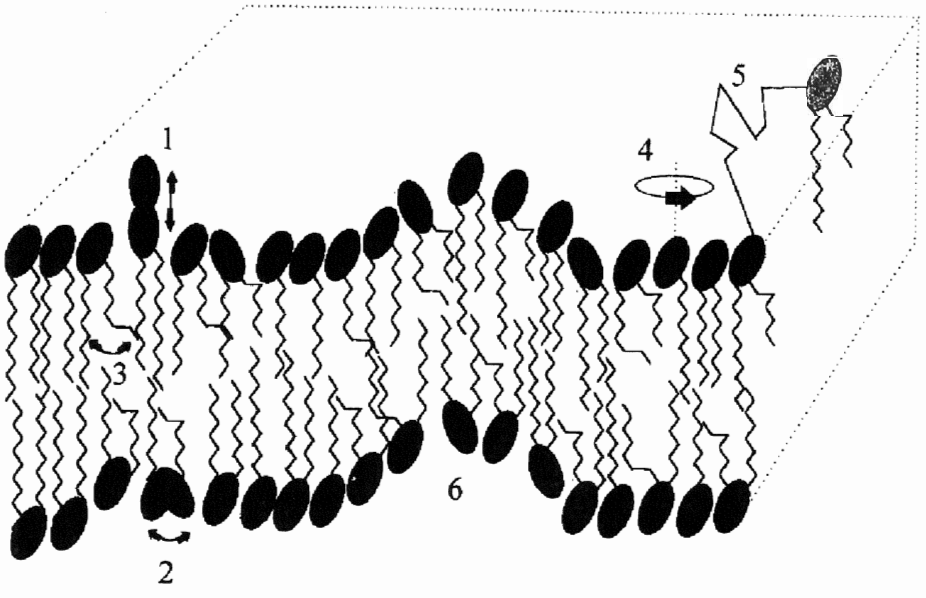

Figure 1.3: Various types of motions present in a fluid bilayer are schematically shown: 1) out-of-plane or vertical vibrational motion of an individual lipid molecule; 2) flip-flop motion of lipid head group; 3) trans-gauche isomerization, or chain defect motions; 4) rotational diffusion of lipid molecules about their director; 5) in-plane or lateral diffusion of lipid molecules; 6) collective undulations of the lipid bilayer. (Reproduced from [17]).

Table 1.1: Some spectroscopies of importance in the study of membranes with their typical ranges and spectroscopic time scales; from Bloom M, Thewalt J. *Chem.Phys.Lipids* **73**, 27-38 (1994).

Excitation	Frequency range	Time scale
Nuclear magnetic resonance (NMR)	10-600 MHz 10^7 to 6×10^8 Hz	10^{-6} to 10^{-4} s for ^{1}H NMR, ^{2}H NMR
Electron spin resonance (ESR) *or* Electron paramagnetic resonance (EPR)	1-300 GHz 10^9 to 3×10^{11} Hz	10^{-8} s
Molecular vibration	6×10^{11} to 3×10^{14} Hz	very short ($< 10^{-10}s$)
Fluorescence polarization	4×10^{14} to 10^{15} Hz	$\approx 10^{-8}s$

membrane systems [32]. The so-called gel-to-liquid crystalline phase transition is a dramatic change in the ability of the individual phospholipid molecules to move. In the frozen or gel state the acyl chains maintain their conformation (bonds do not rotate between gauche and trans orientations). The all-trans state is the preferred conformation at low temperatures. In the higher temperature liquid crystalline state, more energetic conformational states arise which involve one or several trans-gauche isomerizations, and the phospholipid molecules undergo rapid transitions between such states. The molecules form a two-dimensional fluid, with rapid axial reorientations and lateral diffusion responsible for averaging many of the molecular interactions. The gel-to-liquid crystalline phase transition is similar to the ice-water melting transition. For a pure phospholipid-water system this is a sharp transition at a characteristic temperature, T_M. T_M is lowered by shorter acyl chains and by the presence of unsaturation in the acyl chains.

The second type of phase transition in biological or model membrane systems occurs

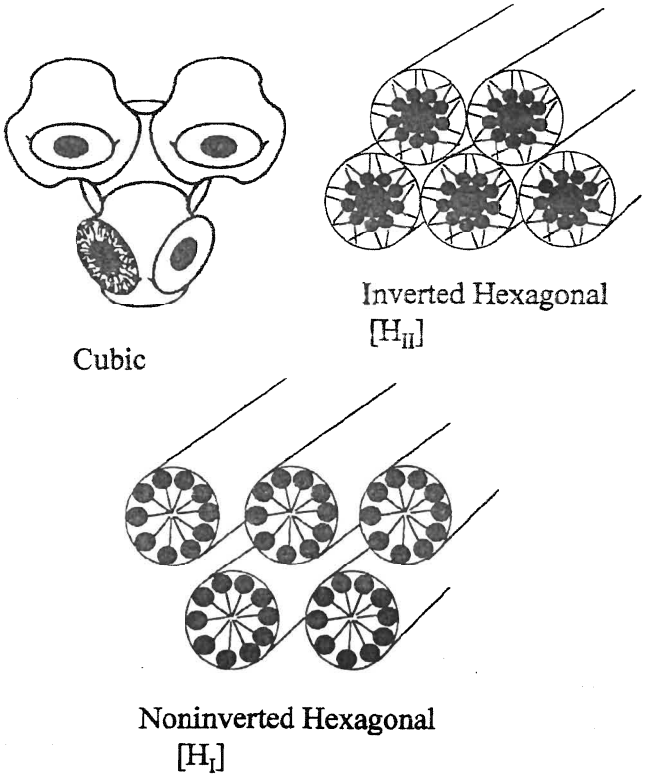

Figure 1.4: The most common non-lamellar phases which can be formed by various lipids. (Reproduced from [17]).

at a characteristic temperature T_H. This type of phase transition involves structural rearrangements of a large number of phospholipid molecules to exclude water from their hydrophobic regions, and thus to minimize water-to-hydrophobic region interaction. This lipid polymorphism can by induced by small changes in temperature, phospholipid composition, non-phospholipid impurities, thermal history, and the presence of a solvent. A variety of such structural phases exists; some are listed in Table 1.2. Figure 1.4. is a schematic representation of possible non-lamellar phases.

Table 1.2: Polymorphs of Phospholipid-Water Systems. Only the most common polymorphs are listed. In all of these phases phospholipids are in a liquid-crystalline state [9].

L_α	Lamellar	Fluid bilayer. Biomembranes take this form (see Fig. 1.2).
C	Cubic	"Plumber's nightmare" arrangement with tubes running orthogonally. There are a number of different cubic phases, the most common being the bicontinuous cubic phase.
H_{II}	Inverted Hexagonal	Tubes of phospholipid with water on the inside, hexagonally packed.
H_I	Noninverted Hexagonal	Tubes of phospholipid with water on the outside, hexagonally packed.

1.4 Lipid Organization and Thermodynamic Properties

A number of physical properties are strongly dependent on the lateral organization and the structural fluctuations of the lipid bilayer. This is particularly true of thermodynamic and thermomechanic response functions, such as specific heat, area compressibility, and bending rigidity, that express the system response due to changes in temperature, surface area, and curvature, respectively. At phase transitions, these response functions display anomalies. Observation of anomalies in response functions has often been taken as a sign of the presence of strong fluctuations and structural reorganizations in the membrane conformation [55].

A large percentage of the phospholipids in natural membranes have one or more double bonds. Presence of unsaturation in the phospholipid chains affects many of the bulk properties of model membrane system. For example, a particular class of monounsaturated lipids exhibit a unique behavior of the phase transition temperatures (gel-to-liquid crystalline T_M and bilayer-to-hexagonal T_H) associated with the position of C=C bond.

Table 1.3: Measured parameters for pure di 18:1 PE lipids. Data from R. Epand, N. Fuller and R.P. Rand, 1996. *Biophys.J.* **71**:1806-1810. ; ‡ - determined by X-ray diffraction; † - from Cullis,P., P.Van Dijck, B. deKruijff, and J.DeGier. 1978. *Biochim.Biophys.Acta.* **513**:21-30.

C=C bond position	T_M (°C)	T_H (°C)
△6 DSPE	16	37
△9 DOPE	-8†	8
△11 DVPE	-1‡	28

As seen in Table 1.3, a strong minimum in both T_M and T_H occurs when the C=C bond is near carbon position 9 in an 18-carbon chain. This work is an attempt to understand the mechanism responsible for these bulk thermodynamic changes. The technique of ^{2}H NMR is used to provide information about the local orientational order of the acyl chains in model membranes.

1.5 Model Membranes in the Magnetic Field

When placed in an external magnetic field molecules may orient due to the presence of an anisotropy in their magnetic susceptibility. For a small molecule the degree of orientation, β, is proportional to the diamagnetic anisotropy, $\triangle\chi$, and to the square of the magnetic field, H [29]

$$\beta = \triangle\chi H^2/k_BT \tag{1.1}$$

where k_B is the Boltzmann constant and T is the temperature. The degree of orientation is usually quite small. However, in a system where diamagnetically anisotropic molecules are held parallel to each other, as in a liquid crystal, the anisotropy is additive and the degree of orientation is also propotional to the number, n, of molecules in the cluster [29]

$$\beta = n\triangle\chi H^2/k_BT \tag{1.2}$$

In high magnetic fields substantial orientation is observed in the liquid crystalline phase [53].The existence of such magnetic distortion in biological and model membranes must be taken into account. It has been shown [35] that such a magnetically induced orientation effect distorts the interpretation of NMR lineshapes.

Chapter 2

Theory of Nuclear Magnetic Resonance

2.1 Classical Introduction

A system with a nonvanishing spin $\vec{S}$ has a magnetic moment $\vec{\mu}$ which is related to $\vec{S}$ by the *gyromagnetic ratio* γ

$$\vec{\mu} = \gamma\hbar\vec{S}. \tag{2.1}$$

Due to the scalar nature of γ we see that $\vec{S}$ and $\vec{\mu}$ are colinear.

A magnetic field $\vec{H}$ influences the magnetic moment, and the resulting torque is

$$\vec{\tau} = \vec{\mu} \times \vec{H}. \tag{2.2}$$

For a static magnetic field $\vec{H} = \vec{H}_0$, the resulting motion is a precession of $\vec{\mu}$ around $\vec{H}_0$ with an angular frequency $\omega_0 = \gamma H_0$, called the *Larmor Frequency* (see Fig. 2.1).

2.2 Quantum Mechanical Description of Motion

In a quantum mechanical picture we can describe the dynamic properties of a spin system with the density operator formalism.

The equations of motion in the presence of a Hamiltonian $\hbar\mathcal{H}$ for the density operator $\mathbf{s}$ are given by

$$\frac{d\mathbf{s}}{dt} = -i[\mathcal{H}, \mathbf{s}]. \tag{2.3}$$

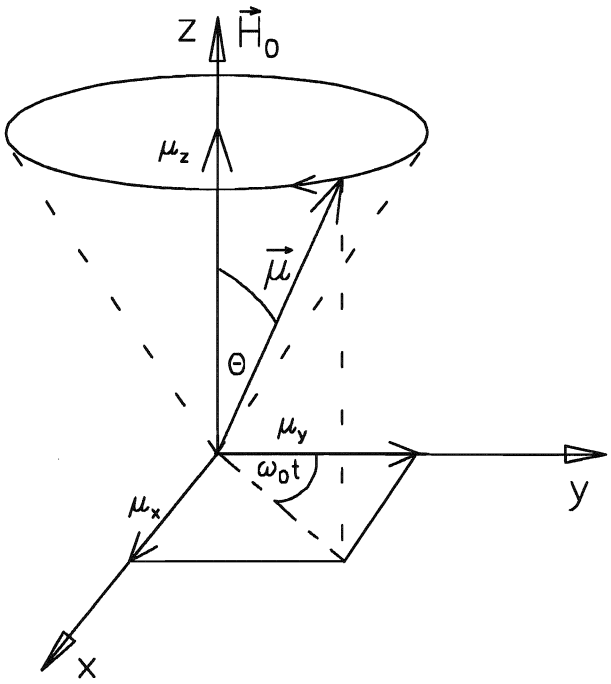

Figure 2.1: Magnetic Top, $\vec{\mu}$ precessing with Larmor Frequency ω_0 around a magnetic field along the z-axis, angle θ is constant for a static field and depends on the initial position of $\vec{\mu}$

Let $\{\mathbf{p_i}\}$ $(i = 1..n,\ \mathrm{Tr}\{\mathbf{p_i p_j}\} = \delta_{ij})$ be a basis set in the space of operators on the Hilbert space of states. Any operator can now be expanded in terms of the basis operators. For example, for the density matrix operator

$$\mathbf{s} = \sum \mathbf{c_i p_i}. \tag{2.4}$$

where c_i are coefficients, informed about the time evolution of the system. If we substitute this expansion in equation 2.3 we get a set of coupled differential equations for the expansion coefficients $c_i = c_i(t)$

$$\frac{dc_i}{dt} = -\sum Q_{ij} c_j, \tag{2.5}$$

where

$$Q_{ij} = -Q_{ji} = -i\mathrm{Tr}\{\mathbf{p_i}[\mathbf{p_j}, \mathcal{H}]\}. \tag{2.6}$$

To calculate the coupling constants Q_{ij} we expand the Hamiltonian in terms of the basis operators and thus reduce the problem to the calculation of the commutators $[\mathbf{p_i}, \mathbf{p_j}]$. A table of these commutator relations for spin $\mathbf{I} = \frac{1}{2}$ and $\mathbf{I} = \mathbf{1}$ can be found in[46].

2.3 Spin-$\frac{1}{2}$ System

For a spin-$\frac{1}{2}$ system $(\mathbf{I} = \frac{1}{2})$, one convenient set of the basis vectors $\mathbf{p_i}$ is given by the *Pauli Matrices* and a unit matrix

$$\mathbf{p_0} = \mathbf{1}, \qquad \mathbf{p_1} = \frac{\mathbf{1}}{\sqrt{\mathbf{2}}}\sigma_\mathbf{x}, \qquad \mathbf{p_2} = \frac{\mathbf{1}}{\sqrt{\mathbf{2}}}\sigma_\mathbf{y}, \qquad \mathbf{p_3} = \frac{\mathbf{1}}{\sqrt{\mathbf{2}}}\sigma_\mathbf{z}. \tag{2.7}$$

In this basis the Hamiltonian for a spin system in a static magnetic field in the z-direction is given by $\mathcal{H} = -\omega_0 \mathbf{p_3}$. Therefore the differential equations for $c_i(t)$ are

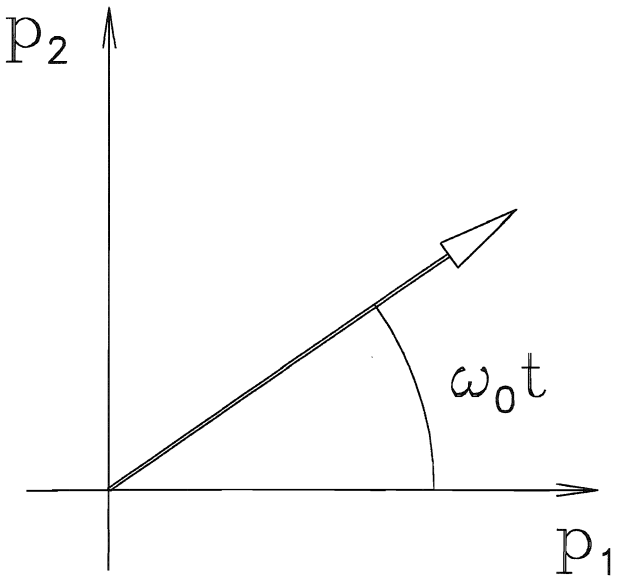

Figure 2.2: Precession diagram for a spin-$\frac{1}{2}$ in a static magnetic field. Coupling between $c_1(t)$ and $c_2(t)$ is shown; c_3 is a constant.

$$\frac{dc_1}{dt} = -\omega_0 c_2, \qquad \frac{dc_2}{dt} = \omega_0 c_1, \qquad \frac{dc_3}{dt} = 0. \tag{2.8}$$

Obviously the solution to these differential equations yields the *Larmor Precession* we already obtained from the classical picture, see the precession diagram in Fig. 2.2.

2.4 Spin-1 System

In a spin-1 system ($\mathbf{I} = 1$) the situation is more complicated. Instead of a two-dimensional spin space we have to deal with a three-dimensional spin space. This leads to a basis set of operators consisting of 9 instead of 4 basis operators. One convenient choice is:

$$\mathbf{p_0 = 1}, \qquad \mathbf{p_1} = \frac{\mathbf{1}}{\sqrt{\mathbf{2}}}\mathbf{I_x}, \qquad \mathbf{p_2} = \frac{\mathbf{1}}{\sqrt{\mathbf{2}}}\mathbf{I_y}, \qquad \mathbf{p_3} = \frac{\mathbf{1}}{\sqrt{\mathbf{2}}}\mathbf{I_z}, \tag{2.9}$$

$$\mathbf{p_4} = \frac{1}{\sqrt{6}}(3\mathbf{I_z}^2 - \mathbf{2}), \qquad \mathbf{p_5} = \frac{\mathbf{1}}{\sqrt{\mathbf{2}}}(\mathbf{I_x I_z} + \mathbf{I_z I_x}), \qquad \mathbf{p_6} = \frac{\mathbf{1}}{\sqrt{\mathbf{2}}}(\mathbf{I_y I_z} + \mathbf{I_z I_y}), \quad (2.10)$$

$$\mathbf{p_7} = \frac{1}{\sqrt{2}}(\mathbf{I_x}^2 - \mathbf{I_y}^2), \qquad \mathbf{p_8} = \frac{\mathbf{1}}{\sqrt{\mathbf{2}}}(\mathbf{I_x I_y} + \mathbf{I_y I_x}).$$

Again, the Hamiltonian for a system with spin 1 in a static magnetic field H_0 can be expressed in terms of the basis operators as $\mathcal{H} = -\sqrt{2}\omega_0 \mathbf{p_3}$. With the help of the commutator table the solution of the set of differential equations for the expansion coefficients $c_i(t)$ can be obtained in exactly the same way as for the spin-$\frac{1}{2}$ system [46]. Unfortunately it is not as easy to visualize the motion of the magnetic moment for a spin-1 system moment as it was for a spin-$\frac{1}{2}$ system. Here we have, besides the coupling of $\mathbf{p_1}$ and $\mathbf{p_2}$ which still yields the Larmor precession, other coupled pairs of basis operators as we can see from the precession diagrams in Figure 2.3.

So far we have only been considering the Zeeman interaction with an external magnetic field. A spin-1 system also possesses a quadrupolar moment eQ which is responsible for a shifting of the Zeeman levels whenever the system is in an electric field gradient (EFG), as depicted in Fig. 2.4. For example, the ^{2}H nuclei (spin-1) of the C-^{2}H (or C-D) bonds in a hydrocarbon molecule where several hydrogen atoms are replaced by deuterium atoms, experience an EFG due to the electrons of the bond. The quadrupolar interaction in this case is relatively small, compared to the Zeeman interaction, and can be treated as a first-order perturbation [46]. In this case the perturbing Hamiltonian is

$$\mathcal{H}_q = \frac{e^2qQ}{4\hbar}(3\mathbf{I_z}^2 - \mathbf{2}) = \sqrt{\frac{\mathbf{2}}{\mathbf{3}}}\omega_\mathbf{q}\mathbf{p_4}, \quad (2.11)$$

where

$$\omega_q = \frac{3}{4}\frac{e^2qQ}{\hbar}. \quad (2.12)$$

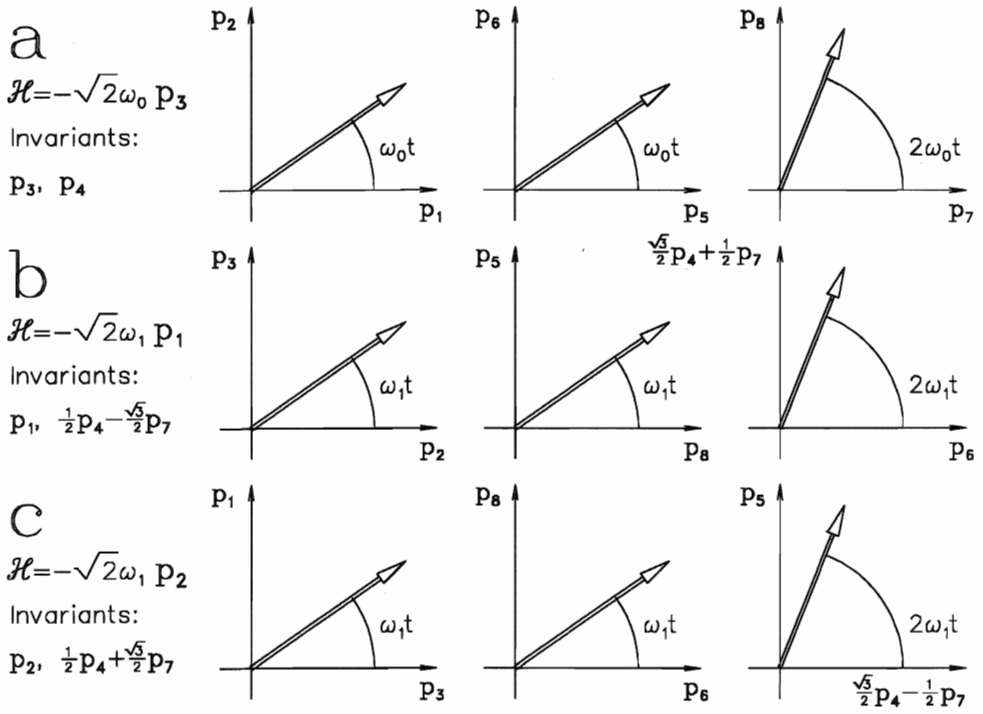

Figure 2.3: Precession diagram for a spin 1 in a static magnetic field. Evolution of $\sigma(t)$ under the Hamiltonians.
(a): $\mathcal{H} = \mathcal{H}_z = -\sqrt{2}\omega_0 \mathbf{p_3}$ (Larmor precession);
(b): $\mathcal{H} = \mathcal{H}_x = -\sqrt{2}\omega_1 \mathbf{p_1}$;
(c): $\mathcal{H} = \mathcal{H}_y = -\sqrt{2}\omega_1 \mathbf{p_2}$.

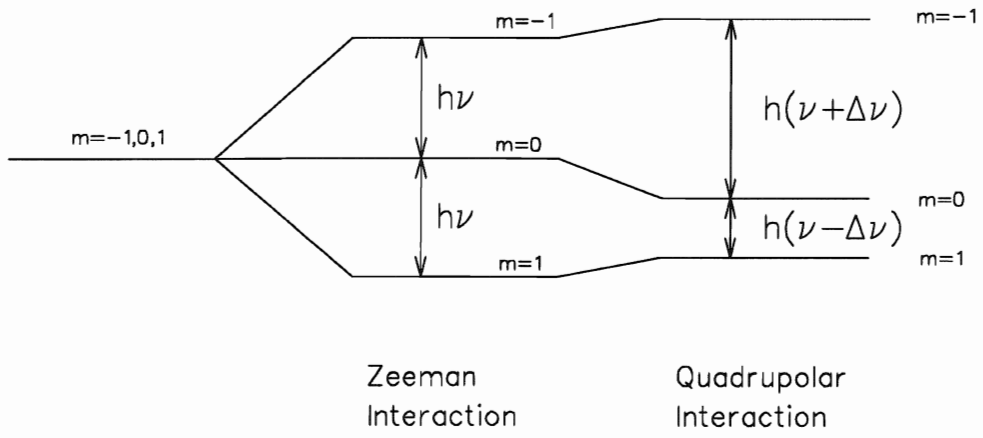

Figure 2.4: Quadrupolar splitting of the Zeeman levels. The energy difference between the m=-1 and the m=0 level is no longer the same as the difference between the m=0 and the m=1 level.

Now the three Zeeman levels get shifted due to the perturbation as illustrated in Fig. 2.4. We see that the energy difference between different levels is not the same any more and we now have two frequencies inducing transitions between the different levels, one frequency slightly lower and one slightly higher than before. The difference between those frequencies is the so-called *Quadrupolar Splitting* which is given by

$$\Delta\nu_q = \frac{3}{8}\frac{e^2qQ}{h}\left[\left(3\cos^2\beta - 1\right) + \eta\cos 2\alpha\sin^2\beta\right], \tag{2.13}$$

where α and β are the Euler angles specifying the orientation of the EFG tensor with respect to the static magnetic field.

From equation 2.13 one sees that the quadrupolar splitting depends on the orientation of the EFG tensor and therefore on the orientation of the C-D bond in the magnetic field. This presents an opportunity to gain information about the orientation and the dynamics of the lipid system by measuring the quadrupolar splitting.

Chapter 3

Measuring Motional Order

3.1 Analytical Description

The motional order (orientational order) of a lipid molecule refers to the degree of motional freedom realized through a particular motion. To quantify the effectiveness of a given motion one normally uses an order parameter. In general, the smaller the value of an order parameter, the greater the number of degrees of freedom experienced by the molecule or molecular segment. Thus in solution, where a molecule experiences extended freedom of diffusional motion resulting in an essentially isotropic motion, the order parameter approaches its smallest value. In contrast, in a crystal where little motion occurs, the molecule is in its most highly ordered state and the order parameter approaches its highest value. The limits of the order parameter depend on its definition, which can change according to the method of measurement. However, the general features of all the order parameters are the same.

Seelig and Seelig [38] have elegantly described the order in terms of molecular parameters. The order parameter for a particular segment of the phospholipid acyl chain can be represented by

$$S_{CD} = P_2(\cos\theta) = \frac{1}{2}\left(3\left\langle\cos^2\theta\right\rangle - 1\right) \tag{3.1}$$

where θ=$\theta(t)$ is the angle a particular chain segment makes at a time t with respect to the bilayer normal, which is the average orientation of the acyl chain as a whole in

the liquid crystalline state. The segmental order parameter is then obtained as a time average of $\theta(t)$, where the average is taken over all motions that modulate θ at rates faster than the spectroscopic time scale. Since S_{CD} is a measure of motional freedom in the vicinity of the given nucleus, it can be used to examine phase changes, relationship between headgroup and acyl tail, effect of cholesterol, protein or peptide, *etc.* on the membrane.

3.2 Methods of Measurement

The observed quadrupolar splitting in a ^{2}H NMR spectrum determined by both the strength of the quadrupolar interaction, well-known for a C-H bond in a hydrocarbon molecule, and the effectiveness of the motional narrowing accompaning rapid molecular motion. Thus, in ^{2}H NMR measurements the order parameter can be derived from a comparison of the measured value of the quadrupole splitting and its well-known static value 167 kHz.

The rate of a given motion determines whether it contributes to the averaging that defines the order parameter S_{CD}. Fast motions will produce motionally narrowed spectra; in biomembranes typical values of S_{CD} are in the range of 0.1-0.2. The descriptions and the scales of the different types of motions is given in Section 1.2.

3.3 Distribution functions $f(y)$ and $p(\theta)$

An essential consequence of the highly symmetric nature of some of the fast motions in model membrane systems is that a spectroscopic observable ω (for example, a quadrupolar splitting) is related to some generalized time-averaged anisotropy parameter y, through the fundamental scaling relationship

$$\omega(\theta) = yP_2(\cos\theta) = \frac{1}{2}y(3\cos^2\theta - 1) \tag{3.2}$$

where θ is the angle between the symmetry axis and the external magnetic field. In general, a system has more than a single inherent time-averaged anisotropy (more than a single order parameter) and thus it is appropriate to introduce an anisotropy distribution function $f(y)$ which contains the physical information of interest. The order parameter profile $S_{CD}(n)$, where n- is the carbon number along the fatty acid chain, of C-D bonds) extracted from the quadrupolar splittings of the ^{2}H NMR spectrum of a phospholipid molecule in a model membrane system, is an example of such a distribution function.

Experimentally, partially ordered systems are often studied using powder samples which contain domains with different orientations, and the observed powder spectrum is a superposition of contributions from all of these orientations. As a result, a single fixed anisotropy parameter y corresponds to a continuous lineshape function, $S_y(\omega)$, in the frequency domain. To determine $S_y(\omega)$ it is essential to consider also the orientation distribution function $p(\theta)$ which represents the probability of encountering a domain oriented at an angle θ with respect to the external magnetic field in a given sample. For an oriented sample (a single crystal), the orientation distribution function reduces to $p(\theta) = \delta(\theta - \theta_0) = \delta(\theta)$ (where for simplicity $\theta_0 = 0$), and the corresponding lineshape is simply $S_y(\omega) = \delta(\omega - y)$. In this case, the position ω of the spectral line is a direct measure of the anisotropy. For a completely random distribution of domains, $p(\theta) = \sin(\theta)$.

Both distribution functions need to be accounted for when considering experimental powder spectra. The following two expressions

$$S(\omega) = \int f(y)[p(\theta)\frac{d\theta}{d\omega}]dy \tag{3.3}$$

$$= \int p(\theta)[f(y)\frac{dy}{d\omega}]d\theta \tag{3.4}$$

represent two equivalent descriptions of the same mapping of the two distribution functions $f(y), p(\theta)$ onto the powder spectrum $S(\omega)$. The two expressions simply reflect which of the two points of view is being taken. Eq. 3.3 is a $f(y)$-weighted superposition of lineshape functions, one for each anisotropy y. On the other hand Eq. 3.4 is a $p(\theta)$-weighted superposition of spectra from the oriented domains which constitute the powder sample, one for each orientation θ. In both cases, ω, y, and θ are related through the fundamental scaling relathinship of Eq. 3.2. Thus, Eq. 3.3 implies $\theta = \theta(y, \omega)$ and Eq. 3.4 implies $y = y(\theta, \omega)$.

3.4 Powder spectrum as a mapping $f(y)$, $p(\theta) \Longrightarrow S(\omega)$

Analysis of the experimental data corresponds to obtaining the inverse of the mapping described by Eq. 3.3 and 3.4, *i.e.* a solution of an integral equation with the kernel function defined in both cases by the expression in the square brackets [35]. Two experimental situations are possible. If $p(\theta)$ is known, and thus an appropriate lineshape function can be calculated, $f(y)$ can be extracted from the powder spectrum. This is precisely the case of "de-Pake-ing" [6], a numerical procedure of extracting an oriented spectrum — and thus, $f(y)$ — from a powder one. Several dePakeing algorithms have been reported and successfully applied to a variety of model and biological membrane systems [6, 45, 54, 30]. DePakeing can also be viewed as an inverse problem. Using the Tikhonov Regularization algorithm [35] for dePakeing allows one to incorporate additional physical information that may be available directly into the data analysis, by modifying the kernel function of Eq. 3.3 [30].

If, instead, $f(y)$ is known, $p(\theta)$ can be determined. An example of such a determination is a measurement of the orientational distribution function of a small guest molecule trapped in the pores of a glassy host, using the chemical shift anisotropies of the guest

molecules, measured separately, as input [37].

Because of the interdependence of ω, y, and θ, it is sometimes possible to determine *both* $f(y)$ and $p(\theta)$ simultaneously, or at least both $f(y)$ and a limited number of parameters which characterize $p(\theta)$ [35]. A generalization of the dePakeing algorithm is made whereby a simple physically reasonable model for $p(\theta)$ is postulated, and then the regularization techniques are used to determine parameters of such a model simultaneously with the reasonable approximation $\tilde{f}(y)$, from the noisy data $S_j^\delta = S_j + \delta_j, j = 1, ..., m$. Restricting the model to a single parameter κ clearly represents the simplest possible case. The expectation is that an effect such as magnetic ordering (see Section 1.4) of model membrane bilayers, for example, can be successfully described by a physically justified one-parameter function $p_\kappa(\theta)$ which approximates the true $p(\theta)$ when the value of κ is chosen appropriately. The parameter κ can be thought to describe the degree of magnetic distortion of the random $p(\theta) = \sin\theta$ distribution. For each fixed value of κ, $p_\kappa(\theta)$ is well-defined and thus $\tilde{f}(y)$ can be determined from the S_j^δ data using the Tikhonov regularization algorithm. Sweeping an appropriate range of values for κ, the minimum of the least-squares error sum (the misfit function)

$$\psi(\kappa) = \sum_{j=1}^{m} [S_j^\delta - S_j(f'(y), \kappa)]^2 \tag{3.5}$$

provides an optimum estimate $\tilde{\kappa}$. Out of all functions $p_\kappa(\theta)$, the one closest to the true $p(\theta)$ is thus determined, leading to the best approximation $\tilde{f}(y)$ within the limits of the model defined by $p_\kappa(\theta)$. This approach is very general and is not restricted to a certain one-parameter model function $p_\kappa(\theta)$. The entire procedure can be repeated using different model functions, in order to determine the best one.

3.5 DePakeing in the Presence of Partial Magnetic Ordering

One example where a need for such a generalized dePakeing method arises, is when bilayer vesicles are deformed by an external magnetic field into non-spherical shapes [29, 8, 44, 21], and the orientational distribution function is no longer random, $p(\theta) \propto \sin\theta$. The effect of the external magnetic field on the distribution of bilayer domain orientations can be considerable [44, 21]. Such ordering distorts the interpretation of NMR spectra. For example, significant errors are introduced if the standard dePakeing procedure is applied to such a partially ordered system [35].

A numerical method of extracting simultaneously the orientational distribution and the oriented spectrum has been proposed [35]. This method which is based on the *Tikhonov Regularisation Algorithm* [52, 18] tests three models for $p(\theta)$.

Ellipsoidal Model :

$$p_E(\theta) \propto \sin\theta \times [1 - (1 - \kappa_E)\cos^2\theta]^{-2} \tag{3.6}$$

This model arises if one considers an ellipsoidal deformation of a spherical assembly. κ_E is the square of the ratio of the semiaxes of the ellipse, $\kappa_E = 1$ returns the undistorted spherical symmetry.

Legendre Model :

$$p_L(\theta) \propto \sin\theta \times (1 + \kappa_L \cos^2\theta) \tag{3.7}$$

Here the correction to $\sin\theta$ is expanded in Legendre Polynominals and truncated after the first two even numbered terms. An infinite series expansion $p_L(\theta) \propto \sin\theta \times \sum_{l=0}^{\infty} \kappa_{L,l} P_l(\cos\theta)$ could represent an arbitrary shape of $p(\theta)$, but it would also leave us with an infinite number of parameters to be determined. Limiting ourselves to the first non-trivial term in the expansion, we obtain the expression of

Eq.3.7. For $\kappa_L = 0$ the distribution function for a randomly distributed sample is regained.

Boltzmann Model :

$$p_B(\theta) \propto \sin\theta \times \exp[\kappa_B \cos^2\theta] \tag{3.8}$$

In the third model the extreme case of a totally uncorrelated orientation of adjacent domains is assumed. A Boltzmann distribution of energies of different domains interacting with the magnetic field is considered, which is proportional to $\cos^2\theta$. Again, $\kappa_B = 0$ yields the random distribution.

For small values of κ_B and of (1-κ_E) the corresponding distributions $p_B(\theta)$ and $p_E(\theta)$ coincide with $p_L(\theta)$. This can be seen if the terms in the square brackets in Eqs. 3.8 and 3.6, respectively, are expanded in $\cos^2\theta$ up to the first order and if one assumes $\kappa_L = \kappa_B = 2(1-\kappa_E)$. Thus, in the limit of a small deviation from the random distribution of orientations, all three models should yield similar results.

As an illustration, an example of such a determination is presented in Chapter 5 of this work, where a ^{2}H NMR spectrum of a PE-lipid and perdeuterated TD mixture exhibits the distortive effect of partial orientational ordering in an applied magnetic field.

3.6 Method of Moments

A method of moments is commonly used to provide information about the spectral lineshape. By definition, the n-th moment about ω_0 of the spectrum with lineshape $g(\omega)$ is

$$M_n(\omega_0) = \frac{\int_{-\infty}^{\infty} d\omega(\omega - \omega_0)^n g(\omega)}{\int_{-\infty}^{\infty} d\omega g(\omega)} \tag{3.9}$$

The first two moments M_1 and M_2 (corresponding to n=1,2) are the most important and commonly used measures of the 'central' value and the mean deviation of the spectrum.

More information about the shape of the spectra can be obtained from higher moments. For example, M_3 measures spectral asymmetry. In the case of a symmetric spectrum all odd moments about the center of symmetry vanish.

In a phase transition, the changing nature of the motional averaging is reflected in the observed spectral changes. Since M_2 is effectively, a measure of the spectral width, a quantitative description of a phase transition in a system can be obtained by calculating the moments of the ^{2}H NMR spectra as a function of temperature [13, 14].

Chapter 4

Materials and Methods

4.1 Materials

The following phosphatidylethanolamines were used in this work: 1,2-Dipetroselinoyl-sn-Glycero-3-Phosphoethanolamine (di-18:1; C=C bond at carbon position 6; refered to as $\triangle 6$ PE in this work); 1,2-Divaccenoyl- sn-Glycero-3-Phosphoethanolamine (di-18:1; C=C bond at carbon position 11; $\triangle 11$ PE) and 1,2-Dipalmitoleoyl- sn-Glycero-3-Phosphoethanolamine (di-16:1; C=C bond at carbon position 9; $\triangle 9$ PE). The lipids were purchased from Avanti Polar Lipids (Alabaste, AL) and used without further purification. The alcohol used was tetradecanol (TD-d_{29}) deuterated in carbon positions 1-14 (98.7 atom % D), obtained from "CDN Isotopes" (PQ): the deuterium-depleted water was obtained from CIL (Andover, MA, USA).

4.2 Sample preparation

Phospholipids and tetradecanol were dissolved separately in 2:1 chloroform:methanol solution and then mixed. The organic solvent was evaporated off, first under a gentle nitrogen gas stream and subsequently, under reduced pressure (10^{-4} torr) for at least two hours. 0.5 mL of deuterium-depleted water was added to the dry sample. Immediately after this, the sample was frozen rapidly in liquid nitrogen and then thawed while being vortexed; this was repeated three times. The resulting dispersions were transferred into glass containers, which were then sealed under argon atmosphere with a teflon plug and

epoxy glue around the edge of the plug. An earlier experiment in which epoxy was not used around the plug, showed a significant loss in the weight of the sample after 4 days of experiments. Presumably this loss occurred through water evaporation. In samples sealed with an epoxy no such loss was observed. All samples were thawed and equilibrated at $+5°C$ at least 1 h before use.

4.3 Spectroscopy

All the spectra were obtained on the home-built spectrometer described elsewhere [47, 48] using an inductively coupled probe, with a 7.05 T magnet corresponding to 46 MHz for deuterium nuclei in the samples. The spectra were obtained using a quadrupolar echo sequence with a τ_{qe} value of $50\mu s$. After the second pulse, 2048 points were collected in quadrature with a dwell time of $5\mu s$. The repetition time of the pulse sequence was 1s. The temperature of the sample was regulated by using a home-built temperature controller based on 'Omega CN 76000' with an effective resolution of 0.1°.

4.4 Software

Three separate models for the orientational distribution function were tested using a computer program based on the Tikhonov regularization algorithm [35]. The details of the algorithm are presented in Chapter 3. All data plots were done using `physica` (Tri-University Meson Facility, Vancouver, BC). The manuscript itself was prepared using LaTeX.

4.5 Orientational Order Parameters from ^{2}H NMR Spectra

A dePaked spectrum is a direct measure of the overall distribution of the order parameter. To assign specific order parameter values to certain carbon positions the following

'integration method' was used [49]. The area of each spectrum was normalized to the total number, the number of ^{2}H nuclei positions in the molecules contributing to the ^{2}H NMR spectra. For a TD-d_{29}, for example, this corresponds to 13 methylene and one methyl group. Therefore, each dePaked spectrum can be viewed as a plot of the number of deuterons per unit interval (σ). If we assume now that σ varies monotonically along the chain, we can assign an average fractional order parameter in each phase to every carbon position n. This is denoted by $\sigma_L(n)$ for the L_α phase and $\sigma_H(n)$ for the H_{II} phase. In practice, often we separately assign the peaks associated with the smallest value of σ to the methyl deuterons. The remaining area under the curve corresponds to 26 deuterons which was divided into 13 equal parts. The value of σ at the center of each of these parts determines the value of $\sigma_L(n)$ and $\sigma_H(n)$ corresponding to the appropriate methylene group in the chain.

An alternative to the 'integration method' is a more traditional direct multiparameter fit to the spectrum. The particular software package that was used in this work, is the so-called 'PERCH' software suite [56]. It is based on the use of integral transforms (IT) for analysis of high-resolution NMR spectra [15]. The main idea of the IT procedure is the following: the frequency-domain spectrum $I(\omega)$ is multiplied with a set of basis functions $f_i(\omega)$, and each product is integrated through the range where its value is nonzero, to produce a set of IT

$$IT_i = \int f_i(\omega) I(\omega) d\omega \tag{4.1}$$

which are then used as the input data for the iterative fitting procedure. The IT method uses a special 'A-shaped' basis function which leads to integral transforms which are very fast to compute and differentiate. Second and principal component regression is used in the calculations of the corrections to the spectral parameters . This IT method allows refinement of 400 unknown parameters at the same time. For example, the frequency,

intensity and line-width of 132 lines can be refined simultaneously together with a 4-term baseline-function. Or, if the linewidth is kept the same for all of the lines, 196 lines can be fitted. A detailed description of the IT method is available elsewhere [15, 23, 24, 25].

Chapter 5

Results and Discussions

5.1 Effect of TD

It has been determined that the addition of alcohol (TD) to the lipid-water mixture lowers the T_H phase transition temperature [16, 27]. With regard to T_M, a similar result has been obtained for positional isomers of 1,2-dioctadecenoyl-sn-glycero-3-phosphocholine [3] and has been explained on the basis of differences in hydrocarbon chain packing [4]. An attempt to explain the differences in T_H among these lipids on the basis of the energetics of the lamellar and hexagonal phases, using studies on the $\triangle 9$ PE is presented in [22].

Since TD has a polar end, it is anchored at the lipid-water interface with its acyl chain extending into the bulk of the lipid. As confirmed in earlier studies of alcohol-lipid-water mixtures [50, 27] we can use TD as a good 'reporter' of orientational order of the acyl chains of the host lipid. We decided to use perdeuterated TD added to the lipid-water mixture since using isotopically labelled lipids is considerably more expensive.

It is well established that the presence of TD lowers the $L_\alpha \rightarrow H_{II}$ phase transition. Since TD is the source of ^{2}H isotopic labels, the higher the concentration of TD the stronger the ^{2}H NMR signal. However, higher concentrations of TD may, in fact, lower T_H below T_M. This overlap with the gel phase would make it impossible to observe the $L_\alpha \rightarrow H_{II}$ transition. In practice, both transition temperatures are lowered by TD, but we do not know in advance by how much. On the other hand, low TD concentration

Table 5.1: Phase transition temperatures for pure PE-lipids and mixture with alcohol. †- from R.Epand, N.Fuller and R.P.Rand. *Biophys.J.* **71**:1806 (1996).

Lipid	T_M (^oC) in pure lipids	T_H (^oC) in pure lipids	T_H (^oC) in mixture		
			17mol $^o/_o$ TD	10mol $^o/_o$ TD	
			heat	heat	cool
△6 DSPE	16†	37†	16-22	16-28	15.5-24.5
△9 DiPoPE		43		5-24	7-20
△11 DVPE	-1†	28†		16-27	15-20

reduces the intensity of the NMR signal.

On the basis of previous experience [49] the first sample was prepared with the compromise concentration 17mol% TD in △6 PE lipids, *i.e.* with C=C in carbon position 6. T_H has been found to be shifted to 16 degrees, which is only one degree above the gel-to-liquid crystalline phase transition in mixture. For this sample (△6 PE + 17mol% TD) the ^{2}H NMR spectra were observed over a range of temperature 11°C-23°C, and the pure lamellar phase has been observed at 16°C while the pure hexagonal phase at 22°C. Thus, the phase transition occurs over a fairly wide range of about 6°C. When the NMR spectra were measured again after a period of three weeks, T_H was observed approximately 2°C lower than in the first set of spectra. In this experiment, gel and L_α phases coexisted and it was impossible to separate the two contributions from each other. Therefore, all future samples were prepared using △6, △9, △11 PE with a TD concentration at 10mol%. The NMR spectra were acquired and phase transitions were observed separately from each other.

The samples were equilibrated at 5°C and then a systematic series of spectra were obtained at ever increasing temperatures ('heating'). At each temperature, the sample was equilibrated for at least one hour before any data was taken. Having reached the highest temperature, another set of spectra was obtained, systematically lowering the

temperature ('cooling') over the same temperature range. The nature of the spectra did not change, but some variation in T_H and T_M were observed. Thus, the behavior of the samples was found to be sensitive to their thermal history. This is in agreement with the results of M.Morrow *et al.* [34] obtained for similar model membrane systems. The temperature range of $L_\alpha \rightarrow H_{II}$ phase transitions were found to be 12°C (16-28°C), 19°C (5-24°C) and 11°C (16-27°C) for $\triangle$6, $\triangle$9 and $\triangle$11 PE, respectively.

Table 5.2 also illustrates that the values obtained from ^{2}H NMR compare well with those obtained by differential scanning calorimetry (DSC). DSC measurements were performed immediately after the sample preparation. The first DSC experiments exhibited slow kinetics of the $L_\alpha \rightarrow H_{II}$ phase transition and suggested a complicated phase behavior on cooling. On heating, a long equilibration at a low temperature (5°C) was determined to be important for obtaining reliable DSC data. The same equilibration was then used during the NMR data acquisition.

The observed difference in T_H temperature as determined from NMR and DSC experiments is probably due to the different equilibration time in these experiments, which for the DSC experiment was only a few minutes compared to one hour for NMR.

5.2 Spectral Analysis

The measured powder spectra of the various ($\triangle$6, $\triangle$9, $\triangle$11) PE lipids with TD-d_{29} at different temperatures are presented in Fig.5.1-5.4. Fig.5.1 and 5.2 show spectra from $\triangle$6 PE lipid at different TD concentrations 17 mol% and 10 mol%. Fig.5.2-5.4 show spectra of $\triangle$6, $\triangle$9, $\triangle$11 PE lipids, consequently, containing 10mol% of TD in each case. All spectra were acquired first while heating and then upon cooling demonstrated a slight hysteresis. Thus, as it was mentioned above, the behavior of the samples was found to be sensitive to their thermal history. The spectra of the pure L_α and H_{II} phases are marked

Table 5.2: T_H and T_M (in°C) measured by NMR and DSC in PE-lipids with 10 mol % TD. † - 0.25 °C/min; ‡ - 1 °C/min.

Lipid	T_H, NMR		T_H, DSC		T_M, DSC	
	heat	cool	heat	cool	heat	cool
△6 DSPE	16–28	15.5–24.5	26-28†	18-22†	12-16†	10-15†
△9 DiPoPE	5–24	7–20	21.7‡	12.4‡	–	–
			20.4†	14.3†	–	–
△11 DVPE	16–27	15–20	17-22‡	10-16‡	–	–
			16-20†			
				12-16†	–	–

on each graph by arrows. In-between, the coexistence of both phases demonstrates a slow process of phase transition. In Fig.5.1 and 5.2 the gel→ L_α phase transition appears at temperatures below 16°, and is absent in Fig.5.3 and 5.4. This means that the gel→ L_α phase transition temperature is shifted below the freezing point for △9 and △11 PE.

L_α lineshapes typically have larger overall splittings. The shape of the spectrum obtained in the H_{II} phase contrasts with that obtained for the L_α phase. The values of quadrupolar splittings in the H_{II} phase are smaller than those for the L_α.

5.3 Moments Analysis

The temperature dependence of the second moment, M_2, for the △6, △9, △11 PE samples is presented in Fig.5.5 A-D. For each case, a slight hysteresis is seen upon heating and cooling. Fig. 5.5A and Fig. 5.5B show the variation of M_2 for the △6 PE samples with different TD concentrations, 17mol% and 10mol%, respectively. For the sample with 17mol% concentration of TD there is a sharp change in M_2 between 13°C and 16°C and between 17°C and 20°C. These changes indicate the phase transitions from gel→ L_α and

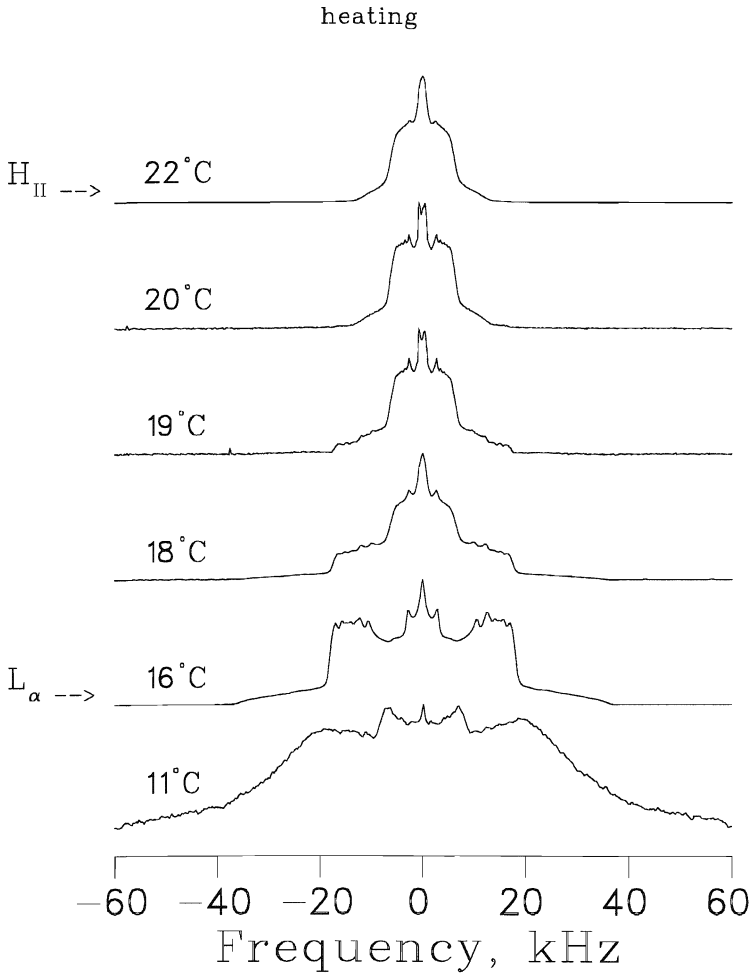

Figure 5.1: L_α and H_{II} phase transition as seen from ^{2}H NMR spectra of $\triangle$6 PE with 17 mol % TD;
the spectrum at 16°C corresponds to the pure L_α phase and at 22°C to the pure H_{II} phase.

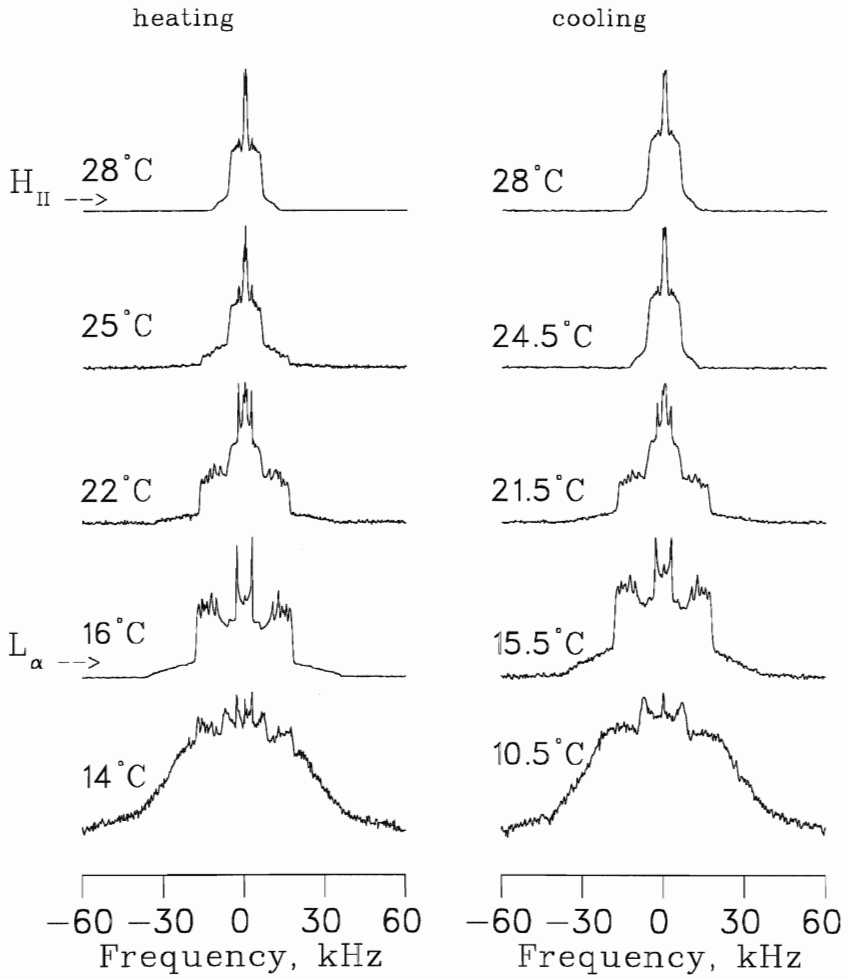

Figure 5.2: L_α and H_{II} phase transition as seen from ^{2}H NMR spectra of $\triangle$6 PE with 10 mol % TD;
the spectrum at 16°C (15.5°C on cooling) corresponds to the pure L_α phase and at 28°C to the pure H_{II} phase.

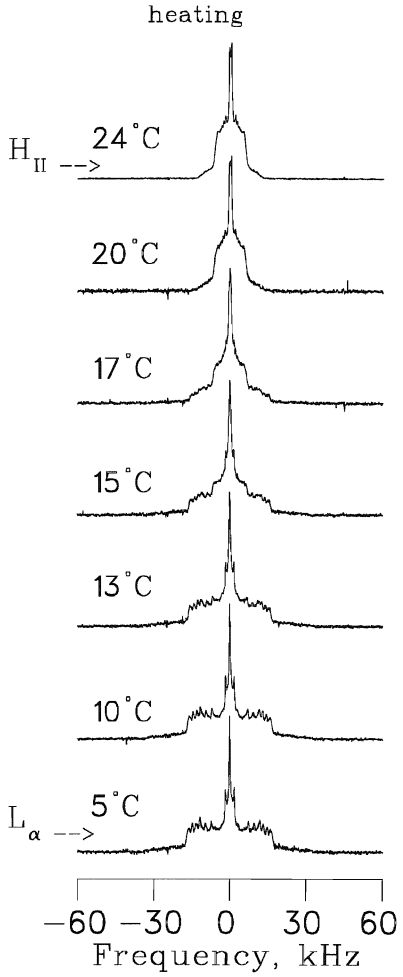

Figure 5.3: L_α and H_{II} phase transition as seen from ^{2}H NMR spectra of $\triangle$9 PE with 10 mol % TD;
the spectrum at 5°C corresponds to the pure L_α phase and at 24°C to the pure H_{II} phase.

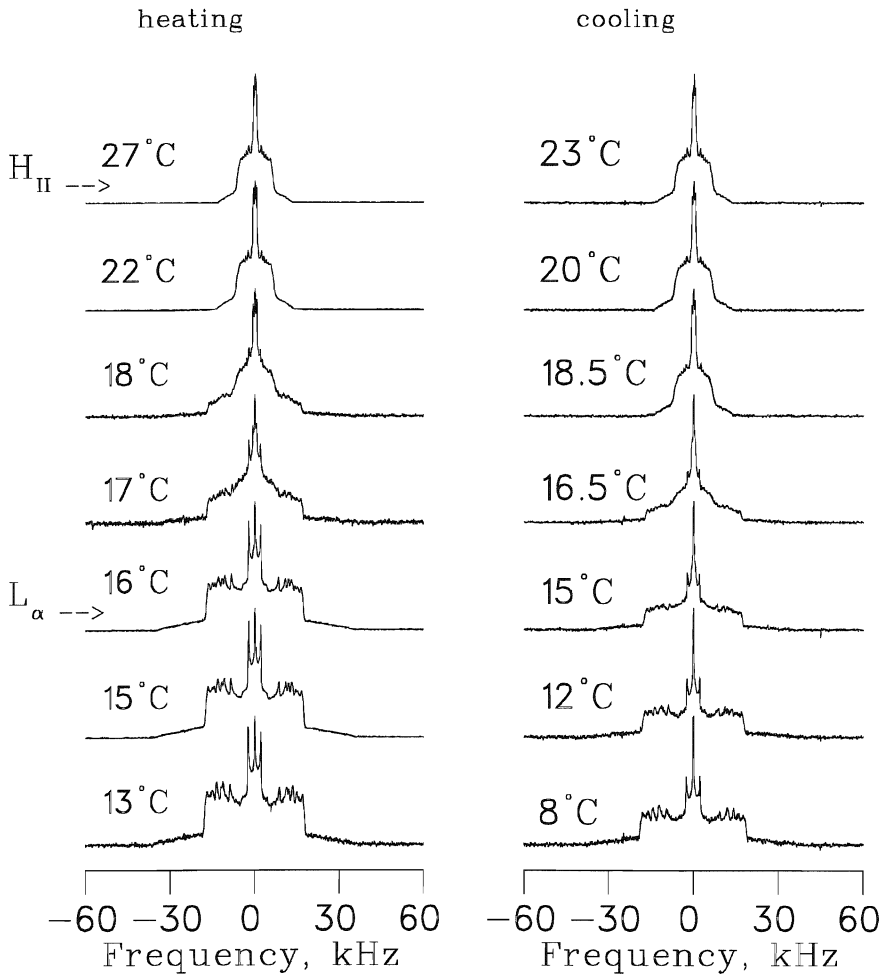

Figure 5.4: L_α and H_{II} phase transition as seen from ^{2}H NMR spectra of $\triangle$11 PE with 10 mol % TD;
the spectrum at 16°C (12°C on cooling) corresponds to the pure L_α phase and at 27°C to the pure H_{II} phase. Note a strong central peak on cooling, in addition to the L_α phase. This is interpreted as evidence of sample deterioration.

$L_\alpha \rightarrow H_{II}$ phases. 16°C has been found to be the only temperature of pure L_α. In the case of 10mol% TD concentration shown in Fig.5.5B, well-defined phase transitions for gel$\rightarrow L_\alpha$ and $L_\alpha \rightarrow H_{II}$ have been found between 7°C and 15°C and between 16°C and 28°C. Fig. 5.5C and Fig. 5.5D show the variation of M_2 for $\triangle$9 and $\triangle$11 PE samples, respectively, but with the same 10mol% TD concentration. The phase transition region from $L_\alpha \rightarrow H_{II}$ is clearly defined on both graphs. For both samples the gel$\rightarrow L_\alpha$ phase transitions have been found to be shifted below the freezing point.

5.4 Comparison of the Orientational Order of the Lipid Chains in L_α and H_{II} phases

The spectra for each of $\triangle$6, $\triangle$9, $\triangle$11 PE samples were dePaked using the Tikhonov regularisation technique [52, 18] and three models (see Section 3.5) were tested for each case in both L_α and H_{II} phases. As an illustration, Fig.5.6 (*top*) shows the misfit function $\Psi(\kappa)$ for each of the three models of $p(\theta)$. Comparing all three curves allows us to select the best one. The lowest minimum of $\Psi(\kappa)$ was determined by the algorithm to be associated with the Legendre model $p_L(\theta)$, and occurs at $\tilde{\kappa}$=-0.07. In our case the depth of the minima in $\Psi(\kappa)$ for the other two models is very similar, suggesting that the other two models also represent the underlying $p(\theta)$ adequately. The shapes of $p(\theta)$ are almost identical in Fig. 5.6 (*bottom*) representing a slight deviation from the random distribution function $p(\theta) = \sin\theta$. The random distribution function, $p(\theta) = \sin\theta$, is also shown in Fig. 5.6 (*bottom*) for comparison. Fig. 5.7A and Fig. 5.8A give an example of measured and recalculated spectra of $\triangle$9 PE sample containing 10mol% TD in H_{II} and L_α phases, respectively. The systematic misfit, as seen in Fig. 5.7A and Fig. 5.8A, essentially disappears. In fact, the presence of a systematic misfit is a reliable indicator of convergence to non-physically oriented spectra, and thus of the inadequacy of a particular

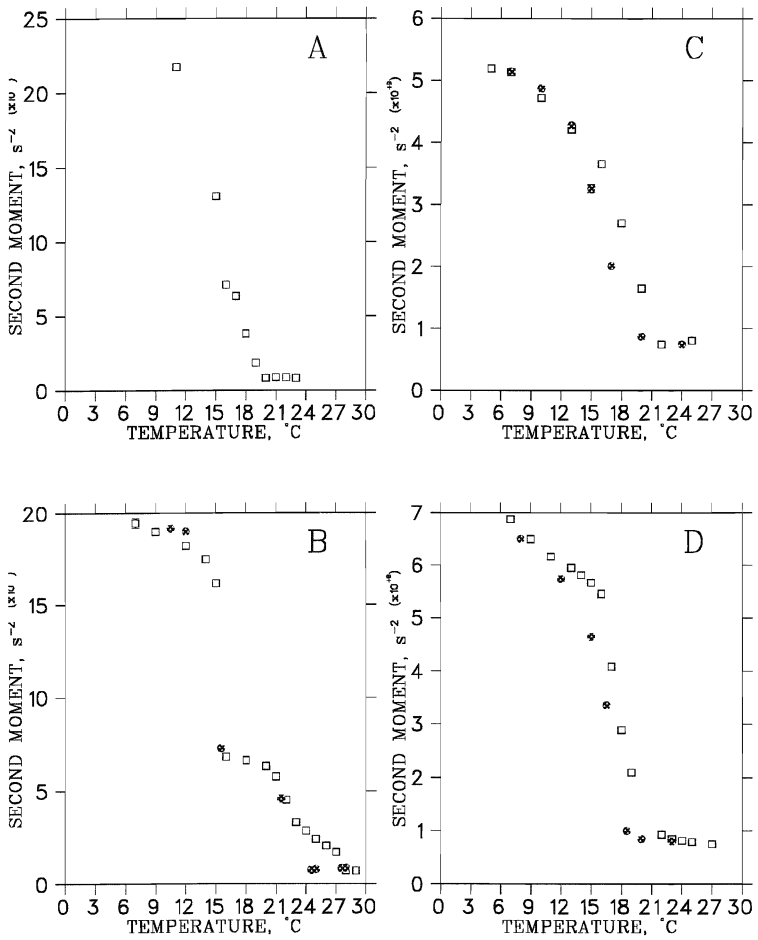

Figure 5.5: The second moment of the spectrum vs. temperature:
(A): △6 DSPE + 17mol% TD; (B): △6 DSPE + 10mol% TD; (C): △9 DiPoPE + 10mol% TD; (D): △11 DVPE + 10mol% TD; □- heating scan and •- cooling scan.

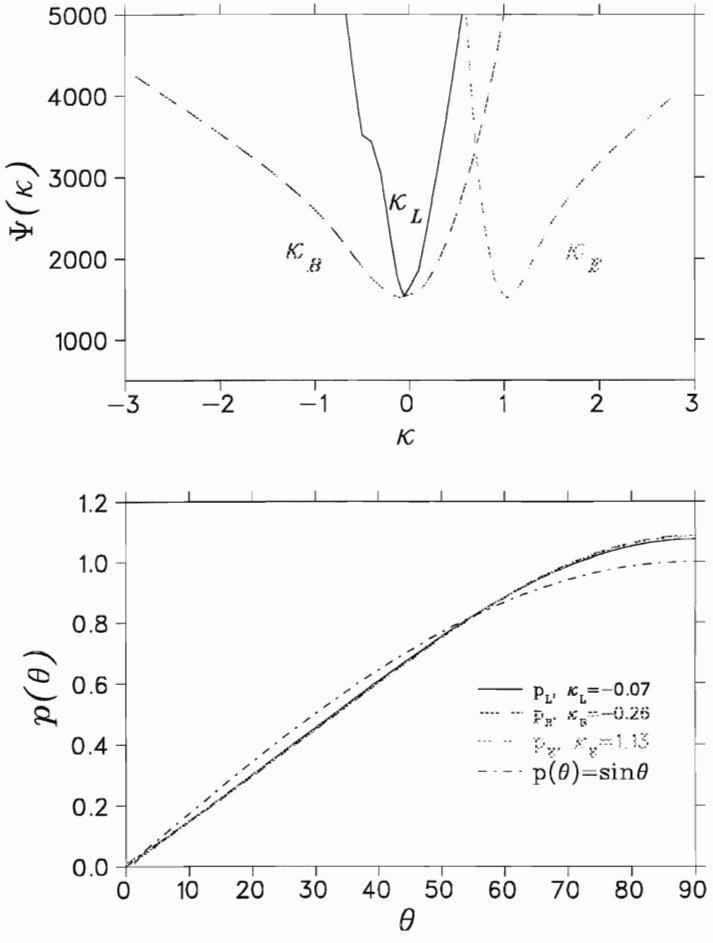

Figure 5.6: *(top)*: Minimizing $\Psi(\kappa)$ yields $\tilde{\kappa}$, for each of the three trial functions $p_L(\Theta)$, $p_B(\Theta)$, and $p_E(\Theta)$. *(bottom)*: three trial orientation dependence functions, calculated for their respective best approximations of $\tilde{\kappa}$, as determined from the three minima above, are shown to illustrate the ability of the algorithm to resolve different shapes of $p(\Theta)$. The random distribution function, $p(\theta) = \sin\theta$, is also shown for comparison.

model being evaluated. This is the reason why a minimum in the misfit function $\Psi(\kappa)$ is used as the criterion for obtaining the estimate $\tilde{\kappa}$. A large systematic misfit even at the minimum of $\Psi(\kappa)$ should be interpreted as a sign that the chosen model for $p(\theta)$ is not adequate [35].

The dePaked spectra (Fig. 5.7B and Fig. 5.8B) obtained from Fig. 5.7A and Fig. 5.8A, respectively, represent a direct measure of the overall distribution of order parameters in the H_{II} and L_α phases. From these spectra, the fractional order parameter for every carbon position was assigned as described in Section 4.5.

The plots of the average $S_{CD}(n)$ values for each phase for the $\triangle 6$, $\triangle 9$ and $\triangle 11$ PE samples are shown in Fig.5.9. The order profiles of the lipid chain is different for the L_α than for the H_{II} phases. For the L_α phase, the characteristic plateau region extends for five/six carbon positions, followed by a rapid decrease of the order toward the end of the lipid chain. In contrast, a more rapid decrease of $S(n)$ with n is observed in H_{II} phase.

Because of the geometry, rapid lateral diffusion of lipid molecules provides an additional degree of motional freedom in H_{II} phase. Rapid lateral diffusion of lipids around the H_{II} cylinders causes additional motional averaging, and leads to a reductoin of the order parameters by a factor of 2 for each carbon position, assuming that the contribution from all other motions remain the same. We can expect this factor of 2 because the lipid diffuses around the cylindrical axes in a time short on the NMR time scale, which projects the symmetry axis for the orientational order from the local surface normal to the axis of symmetry of the cylinder, which is at right angles to the surface normal. Thus, $|\langle P_2(\cos\theta)\rangle| = \left|\left\langle \frac{3\cos^2 90°-1}{2}\right\rangle\right| = \frac{1}{2}$ when the average is taken over motions with a single axis of cylindrical symmetry.

In our case (see Fig. 5.9), firstly, the decrease of orientational order reaches the value of 2.8 for some carbon positions instead of expected factor of 2 for each of them. This result indicates that the H_{II} phase is characterized by more motional freedom of the lipid

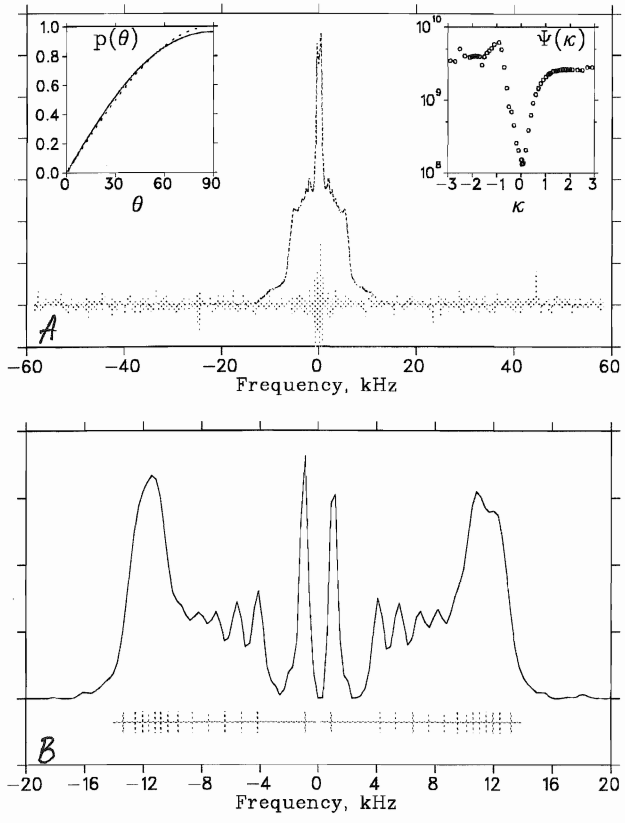

Figure 5.7: (A:) ^{2}H NMR spectrum of $\triangle$9 PE+10mol% TD in H_{II} phase, dePaked using Legendre model; *(solid line)* the measured spectrum; *(dotted line)* the recalculated spectrum and misfit (x10) at the bottom. Insertion on the left: orientational distribution function $p(\Theta)$; the dotted line is the random distribution $p(\Theta) \propto \sin\Theta$, the solid line is the calculated orientational distribution $p_L(\Theta)$. Insertion on the right: $\Psi(\kappa)$ over k, where $\Psi(\kappa)$ is the integral over the squared misfit. The minimum is at κ_L=-0.07.
(B): *(solid line)* DePaked spectrum. *(ticks on the bottom)* The fractional order parameter for each carbon position is assigned by calculating the midpoint of integrals weighted 3-2-2-2-...., as discussed in section 4.5. Their locations are shown below the spectrum.

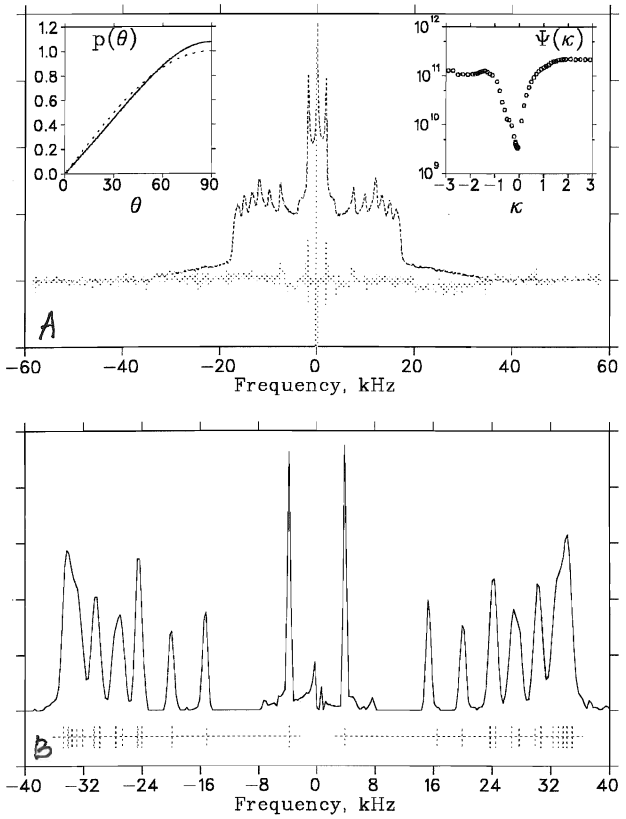

Figure 5.8: (A:) ^{2}H NMR spectrum of $\triangle$9 PE+10mol% TD in L_α phase, dePaked using Legendre model; *(solid line)* the measured spectrum; *(dotted line)* the recalculated spectrum and misfit (x10) at the bottom. Insertion on the left: orientational distribution function $p(\Theta)$; the dotted line is the random distribution $p(\Theta) \propto \sin\Theta$, the solid line is the calculated orientational distribution $p_L(\Theta)$. Insertion on the right: $\Psi(\kappa)$ over κ, where $\Psi(\kappa)$ is the integral over the squared misfit. The minimum is at κ_L=-0.07.
(B): *(solid line)* DePaked spectrum. *(ticks on the bottom)* The fractional order parameter for each carbon position is assigned by calculating the midpoint of integrals weighted 3-2-2-2-...., as discussed in section 4.5. Their locations are shown below the spectrum.

chain than we expected. Secondly, the decrease of orientational order in H_{II} phase do not express by a single scalling factor along the acyl chain. These changes are consistent with the change in geometry of the spacing available for the acyl chain motion resulting from the phase transition. Since we want to characterize the systematic variation of S_{CD} with chain position n across the phase transition, the ratio of the order parameter $S_{CD}(n)$ in the H_{II} phase to that in the L_α phase can provide more information on chain packing. Some of the discrepancy is likely due to the fact that all of the molecular motions are strongly temperature-dependent, and the spectra for pure L_α and H_{II} phases are measured at temperatures several degrees apart, as the transition is fairly broad.

To emphasize the systematic variation in conformational averaging along the chain we use the ratio

$$R(n) = \frac{\sigma_H(n)}{\sigma_L(n)}, \tag{5.1}$$

where $\sigma_H(n)$ and $\sigma_L(n)$ are normalized fractional order parameters in the H_{II} and L_α phases, respectively. This ratio should, in principle, be determined from coexisting spectra obtained at a common temperature. But since we are unable to separate the coexisting spectra exactly in the middle of the phase transition, we calculate the values of $R(n)$ under the assumption that the L_α and H_{II} spectra approximately scale with temperature, *i.e.* that $\sigma_H(\mathrm{n})/(\sigma_H)_{max}$ and $\sigma_L(\mathrm{n})/(\sigma_L)_{max}$ do not change appreciably for a small change in temperature. Therefore, we approximate $R(n)$ by the ratio $\sigma'_H(n)/\sigma'_L(n)$, where σ'_H and σ'_L are measured from the spectra of the pure H_{II} and L_α phases in Fig.5.7A-Fig.5.8D.

The resulting plots of $R(n)$ versus n for the $\triangle$6, $\triangle$9 and $\triangle$11 PE samples and with 10mol% TD are presented in Fig.5.10. Where, order parameter profiles were first normalized by their respective $\sigma(1)$, and then their ratios $R(n)$ were calculated. Lines connecting data points indicate groups of unresolved peaks in the dePaked spectra. The same lipids with two different concentrations of TD (17mol% and 10mol%) exhibit no

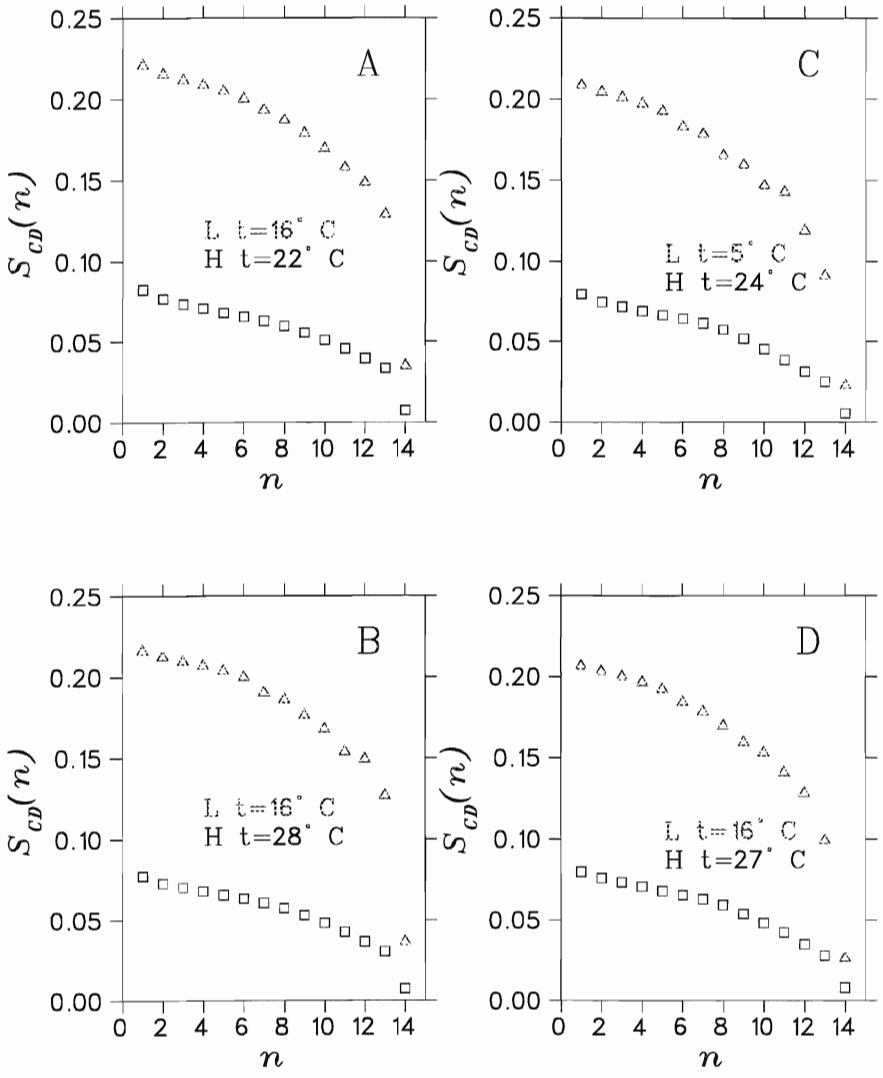

Figure 5.9: Order parameter profiles of L_α (△) and H_{II} (□) phases.
(A): 17 mol% TD + DSPE at 6;
(B): 10 mol% TD + DSPE at 6;
(C): 10 mol% TD + DiPoPE at 9;
(D): 10 mol% TD + DVPE at 11.

difference in the order parameter profiles and, hence, these results are not presented.

All three plots indicate that the order profiles are sensitive to the presence of the double-bond. Subtle changes are seen in the profiles near C=C bond position.

It has been reported previously that the order parameter profile of $\triangle 9$ PE-lipids probed with perdeuterated TD exibit an almost linear decrease of $R(n)$ to the first nine points [49]. The results of the present work appear to contradict those obtained earlier. The most likely explanation of this discrepancy is that in the present work a new algorithm for determination of the orientational order parameter was used. This algorithm took into account the magnetically-induced distortion of the orientational distribution function $p(\theta)$. It has been reported that the subtle changes in the order parameter profiles represented by $R(n)$ are comparable in magnitude to those due to the errors introduced by the dePakeing procedure, if the magnetic distortion of $p(\theta)$ is not taken into account.

5.5 Lineshape analysis of dePaked spectra

The result obtained in the previous section demonstrates that the order parameter profile can be obtained from the dePaked spectra using the 'integration method' described in Section 4.5. Since some of the individual peaks in the dePaked spectrum are not resolved, we cannot unambiguously determine the quadrupolar splittings associated with these specific positions on the chains. For example, in the case of $\triangle 9$ PE sample (see Fig.5.10), we cannot resolve peaks associated with $n = 1, ...9$ and $n = 10, ...12$. We can only make general observations about the behavior of the order parameter profile. To verify that the observed effect was not an artifact of the 'integration method', a direct lineshape fit to the dePaked spectra was performed. A comparison of the order parameter profiles obtained using these two different methods is presented in Fig.5.11-5.13. The results are

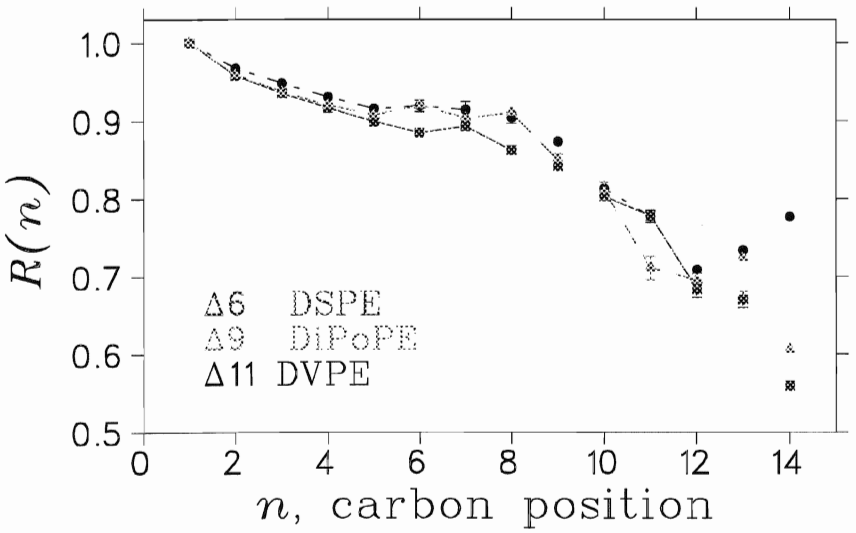

Figure 5.10: Ratio of the fractional order parameters in the L_α and H_{II} phases. (□): Δ6 DSPE + 10mol% TD; (△): Δ9 DiPoPE + 10mol% TD; (○): Δ11 DVPE + 10mol% TD. Lines connecting data points indicate groups of unresolved peaks in the dePaked spectra.

consistent with one another, confirming that Fig 5.10 is indeed, representative of the changes in the order parameter taking place in a $L_\alpha \rightarrow H_{II}$ phase transition.

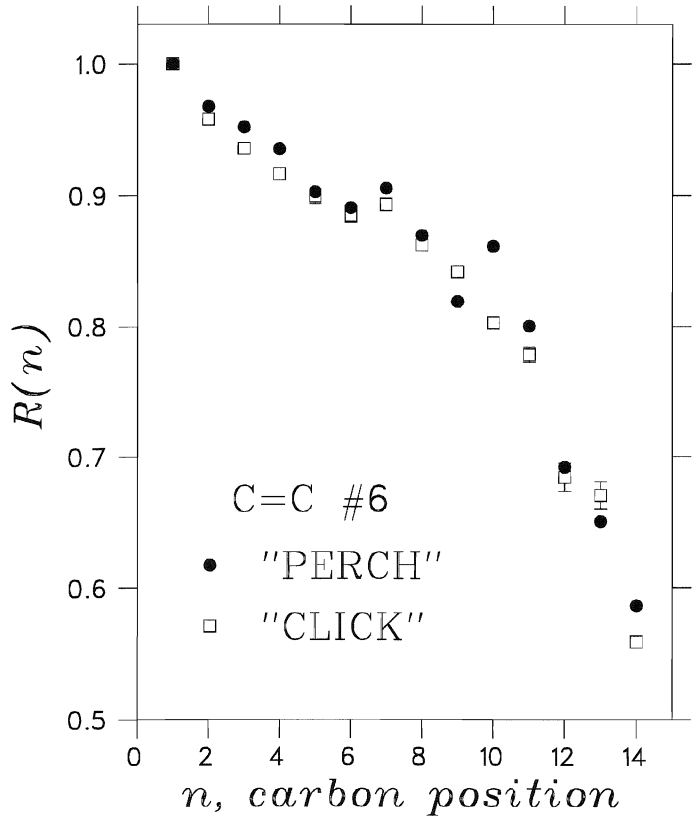

Figure 5.11: Comparison of the order parameter profiles obtained from the direct line-shape fit ('PERCH') and the 'integration method' ('`click`') for $\triangle 6$ PE sample with 10mol% TD.
The error bars represent random errors; if not seen, they are smaller than the size of the plotting symbols.

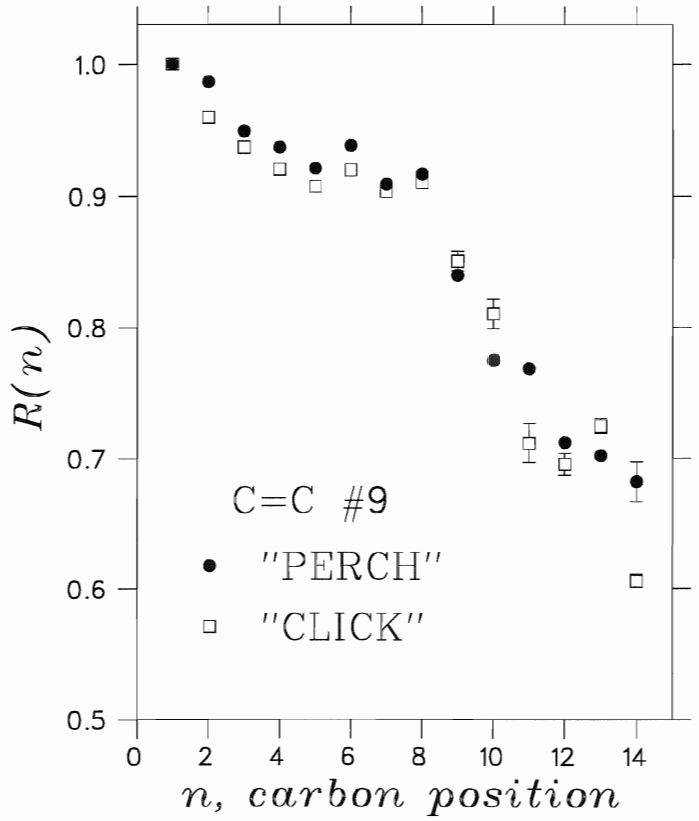

Figure 5.12: Comparison of the order parameter profiles obtained from the direct lineshape fit ('PERCH') and the 'integration method' ('`click`') for $\triangle 9$ PE sample with 10mol% TD.
The error bars represent random errors; if not seen, they are smaller than the size of the plotting symbols.

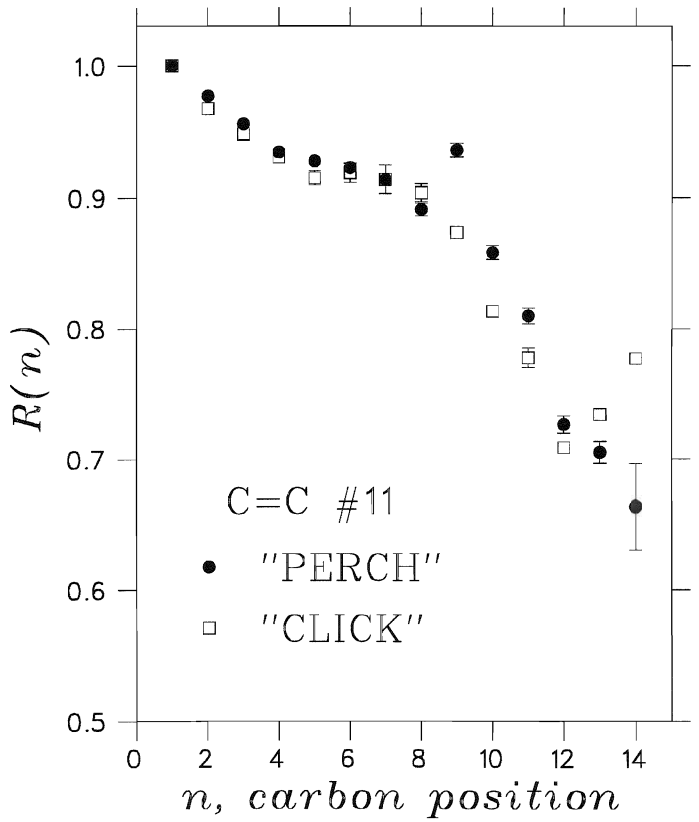

Figure 5.13: Comparison of the order parameter profiles obtained from the direct lineshape fit ('PERCH') and the 'integration method' ('`click`') for $\triangle 11$ PE sample with 10mol% TD.
The error bars represent random errors; if not seen, they are smaller than the size of the plotting symbols.

Concluding Remarks

The order parameter distribution along the fatty acid chain of monounsaturated phospholipids in a model membrane system is seen to be more uniform for the H_{II} phase than for the L_α. This is illustrated directly by the dePaked results (Fig.5.7B,5.8B) or by the order parameter profile for which a continuous decrease of $S_{CD}(n)$ versus n was observed (Fig.5.10).

The same lipids with two different concentrations of TD (17mol% and 10mol%) exhibit little difference in the order parameter profiles.

The orientational order parameter profile of the acyl chain is sensitive to the location of the double-bond. Near the C=C bond position a 'kink' in $R(n)$ is seen on Fig.5.11-Fig.5.13. One of the most important conclusions that can be drawn from this work, is that all three samples (see Fig.5.11-Fig.5.13) reveal a local increase ('kink') in the values of the order parameter associated with the presence of the C=C bond in the lipid chains. This local *increase* in order, associated with chain unsaturation, can be thought of as a local decrease in motional freedom, *i.e.* locally the lipid chain becomes more rigid.

The question of how a local increase in order, associated with a C=C bond, affects the structural reorganization of the lipid phase remains unresolved. It is evident that the inclusion of the C=C bond is critical for structural reorganization of the lipid chain [19, 31, 43] and that such reorganization corresponds to an overall *decrease* in orientational order. A detailed information on such *lowering* of the chain order by a single C=C bond was presented by A.Seelig in 1977 [40]. In addition, the data from [41] suggests that the largest changes in membrane organization caused by unsaturation are observed after incorporation of the first two C=C bonds per chain. Increasing the number of C=C

bonds has a selective effect and preferentially reduces the order in the lower part of the lipid chain close to the methyl group [41]. The greater changes in order toward the middle of the chain with increasing unsaturation suggest a change in the structural geometry of the lipid chain [20]. A separate, and puzzling observation is that when proteins are included in bilayers, they have almost no effect on the packing of the chains as measured by ^{2}H NMR [33, 51].

The order parameters profiles describe how the flexibility of the molecule varies along the chain, and it is not surprising that we observe a local ordering effect, associated with a C=C bond. On the other hand, we also see that unsaturated lipids are more disordered overall than saturated ones at equal absolute temperature, in agreement with other measurements [40, 2]. The absolute values of the order parameters, obtained in the present work, are generally smaller than those for the saturated lipids. Thus, on the one hand unsaturation introduces order in the system locally, but on the other hand it reduces the absolute values of the order parameters overall.

In this work for the first time a new method was used to elucidate subtle effects in the order parameter profiles associated with unsaturation. This method takes into account the distortion of the membrane shape by an external magnetic field. The two effects are comparable in terms of their influence on the NMR spectra, and must both be accounted for. It seems likely that further understanding of the effect of unsaturation requires that a motional model defining the geometry of the chain packing is defined. The $\triangle 9$ lipid (C=C bond at ninth carbon) reveals a dramatic change in T_H, which corresponds to a dramatic reduction in order at a much lower temperature. This may represent a specific geometry of the chain packing. However, the results of our work do not reveal the significant difference in the order parameter profiles between the $\triangle 6$, $\triangle 9$, $\triangle 11$ PE lipids (see Fig. 5.10.). This is probably due to the indirect nature of the measurement in which a guest molecule (TD) was used to report on the motional order of the host lipids.

As we expected, TD is anchored at the lipid-water interface by its polar end, but slight variations in the exact depth of TD along the hydrocarbon chain of the lipid are likely. As was discussed previously [27], the use of TD gives an effective, 'smoothed', shape of the order parameter profile that might not reveal the detailed structure of the molecular order parameter profile. For example, a slight shift in the position of the TD molecule would correspond to a significant systematic error in the order attributed to the host lipids. Therefore, some crucial local variations which may exist in the order parameter profile are not accurately reproduced.

Better resolution would be obtained if deuterated lipids were used as a probe of the C=C bond. In order to examine the correlation between the two different probes of the C=C presence, it is of interest to compare the profiles obtained for the TD/PE-lipid system using deuterated lipid and deuterated alcohol. This might become the next logical step of this work.

Bibliography

[1] Abragam A. Principles of Nuclear Magnetism. Oxford University Press, London, 1961.

[2] Barry J.A., Trouard T.P., Salmon A. and Brown M.F. Low temperature ^{2}H NMR spectroscopy of phospholipid bilayers containing docosahexaenoyl (22:6w3) chains. *Biochemistry* **30**:8386, 1991.

[3] Barton P.G., and Gunstone F.D. Hydrocarbon chain packing and molecular motion in phospholipid bilayers formed from unsaturated lecithins. *J.Biol.Chem.* **250**:4470, 1975.

[4] Berde C.B., Andersen H.C. and Hudson B.S. A theory of the effect of head-group structure and chain unsaturation on the chain melting transition of phospholipid dispersions. *Biochemistry* **19**: 4279, 1980.

[5] Bloom M., Davis J.H., and Dahlquist F.W. Determination of orientational order in bilayer systems using moments of deuterium magnetic resonance spectra. XXth Ampere Congress, Tallinn, Estonia, August 1978

[6] Bloom M., Davis J.H., and MacKay A.L. Direct determination of the oriented sample NMR spectrum from the powder spectrum for systems with local axial symmetry. *Chem. Phys. Lett.* **80**:198, 1981.

[7] Bloom M. and Thewalt J. Spectroscopic determination of lipid dynamics in membranes. *Chem. Phys. Lipids* **73**:27, 1994.

[8] Boroske E. and Helfrich W. Magnetic anisotropy of egg lecithin membranes. *Biophys. J.* **24**:863, 1978.

[9] Cleve R. *Role of 10- and 14-carbon alkanes in H_{II} phase of DOPE.* M.Sc.thesis, Department of Physics, Brock University, 1997.

[10] Cullis P., Farren B. and Hope M. ^{31}P NMR techniques and membrane lipid structure: implications for mechanisms of membrane fusion. *Canadian J. Spectroscopy* **26**:89, 1981.

[11] Davis J.H. The decription of lipid membrane conformation, order and dynamics by ^{2}H NMR. *Biochim. Biophys. Acta* **737**:117, 1983.

[12] Davis J.H. and Jeffrey K.R. The temperature dependence of chain disorder in potassium palmitate-water. A deuterium NMR study. *Chem. Phys. Lipids* **20**:87, 1977.

[13] Davis J.H., Maraviglia B., Weeks G. and Godin D.V. Bilayer rigidity of the erythrocyte membrane. ^{2}H-NMR of a perdeuterated palmitic acid probe. *Biochim. Biophys. Acta* **550**:362, 1979.

[14] Davis J.H., Nichol C.P., Weeks G. and Bloom M. A study of the cytoplasmic and outer membranes of Escherichia coli by deuterium magnetic resonance. *Biochemistry* **18**:2103, 1979.

[15] Diehl P. and Vogt J. Automatic Analysis of n.m.r. Spectra; A Practical Application to the Spectra of Oriented 2,4-Dichlorobenzaldehyde and 2-Chlorobenzaldehyde. *Org. Magn. Reson* **8**:638, 1976.

[16] Epand R., Fuller N. and Rand P. Role of the Position of Unsaturation on the Phase Behavior and Intrinsic Curvature of Phosphatidylethanolamines. *Biophys. J.* **71**:1806, 1996.

[17] Gaulin B.D and Katsaras J. Neutron scattering from soft hydrogenous materials. *Physics in Canada* **53**:247, 1997.

[18] Groetsch C.W. The theory of Tikhonov regualarization for Fredholm Equations of the first kind. Pitman, London, 1984.

[19] Gruner S.M. Intrinsic curvature hypothesis for biomembrane lipid composition: A role for nonbilayer lipids. *Proc. Natl. Acad. Sci. USA* **82**:3665, 1985.

[20] Holte L.L., Peter S.A., Sinnwell T.M. and Gawrisch K. ^{2}H NMR order parameter profiles suggest a change of molecular shape for phosphatidylcholines containing a polyunsaturated acyl chain. *Biophys. J.* **68**:2396, 1995.

[21] Jansson M., Thurmond R.L., Trouaard P. and Brown M. Magnetic alignment and orientational order of dipalmitoylphosphatidylcholine bilayers containing palmitoyllysophosphatidylcholine. *Chem. Phys. Lipids* **54**:157, 1990.

[22] Kozlov M.M., Leikin S., Rand R.P. Bending, hydration and void energies quantitatively account for the hexagonal-lamellar-hexagonal reentrant phase transition in dioleoylphosphatidylethanolamine. *Biophys. J.* **67**:1603, 1994.

[23] Laatikainen R. Automated Analysis of NMR Spectra. *J.Magn.Reson.* **92**:1, 1991.

[24] Laatikainen R., Niemitz M., Weber U., Sundelin J., Hassinen T. and Vepsalainen J. General strategies for Total-Line-Shape type spectral analysis of NMR spectra using Integral Transform. *J. Magn. Reson.* **A120**:1, 1996.

[25] Laatikainen R. Computational strategy for Deconvolution of NMR spectra with with multiplet structures and constraints: analysis of overlapping 13C-2H multiplets of 13C enriched metabolites from cell suspensions incubated in deuterated media. *Magn. Reson. Med.* in press.

[26] Lafleur M., Fine B., Sternin E., Cullis P. R. and Bloom M. Smoothed orientational order profile of lipid bilayers by ^{2}H-nuclear magnetic resonance. *Biophys. J.* **56**:1037, 1989.

[27] Lafleur M., Cullis P.R., Fine B. and Bloom M. Comparison of the Orientational order of Lipid Chains in the L_α and H_{II} Phases. *Biochemistry* **29**:8325, 1990.

[28] Mantsch H.H., Saito H. and Smith I.C. Deuterium magnetic resonance: applications in chemistry, physics and biolody. *Prog. NMR Spectrosc.* **11**:211, 1977.

[29] Maret G. and Dransreld K. Macromolecules and membranes in high magnetic fields. *Physica* **86-88B**:1077, 1977.

[30] McCabe M.A. and Wassall S.R. Fast-fourier-transform dePaking. *J. Magn. Reson. B* **106**:80, 1995.

[31] Mitchell D.C., Straume M. and Litman B.J. Role of sn-1-saturated, sn-2-polyunsaturated phospholipids in control of membrane receptor conformational equilibrium: Effect of cholesterol and acyl chain unsaturation on the metarhodopsin I-metarhodopsin II equilibrium. *Biochemistry* **31**:662, 1992.

[32] Molecular Biology of the Cell. 2-d edition, 1989.

[33] Monck M.A., Bloom M., Lafleur M., Lewis R.N.A.H., McElhaney R.N. and Cullis P.R. Influence of lipid composition of the orientational order in *Acholeplasma laidlawii* strain B membranes: A deuterium NMR study. *Biochemistry* **31**:10037, 1992.

[34] Morrow M.R., Davis P.J., Jackman C.S. and Kevin M.W. Thermal history Alters Cholesterol Effect on transition of 1-palmityl-2-linoleoyl Phophatidylcholine. *Biophys. J.* **71**:3207, 1996.

[35] Schäfer H., Madler B. and Sternin E. Determination of Orientational order parameters from ^{2}H NMR spectra of magnetically partially oriented lipid bilayers. *Biophys. J.* **74**:1007, 1998.

[36] Schäfer H. and Sternin E. Inverse ill-posed problems in experimental data analysis in physics. *Physics in Canada* **53**:77, 1997.

[37] Schäfer H. and Stannarius M. Calculation of orientational distributions of partially ordered samples from NMR spectra. *J. Magn. Reson. B* **106**:1423, 1995.

[38] Seelig A. and Seelig J. The dynamic structure of fatty acyl chains in a phospholipid bilayer measured by deuterium magnetic resonance. *Biochemitry* **13**:4839, 1974.

[39] Seelig A. and Seelig J. Bilayers of dipalmitoyl-3-sn-phosphatidylcholine conformational differences between the fatty acyl chains. *Biochim. Biophys. Acta* **406**:1, 1975.

[40] Seelig A. and Seelig J. Effect of a single *cis* double bond on the structure of a phospholipid bilayer. *Biochemistry* **16**:45, 1977.

[41] Separovic F. and Gawrisch K. Effect of Unsaturation on the Chain Order of Phosphatidylcholines in a Dioleoylphosphatidylethanolamine Matrix. *Biophys. J.* **71**:274, 1996.

[42] Singer S.J. and Nicolson G.L. *Science* **175**:720, 1972.

[43] Slater S.J., Kelly M.B., Taddeo F.J., Ho C., Rubin E. and Stubbs C.D. The modulation of protein kinase C activity by membrane lipid bilayer structure. *J. Biol. Chem.* **269**:4866, 1994.

[44] Speyer J., Sripada P.K., Das Gupta S.K., Shipley G.G. and Griffin R.G. Magnetic orientation of sphingomyelin-lecithin bilayers. *Biophys. J.* **51**:687, 1987.

[45] Sternin E. and Bloom M. Depaking of NMR spetra. *J. Magn. Reson.* **55**:274, 1983.

[46] Sternin E. Some mechanism of transverse NMR in model membranes. PhD thesis, Department of Physics, UBC, 1988.

[47] Sternin E. Data acquisition and processing: A system approach. *Rev. Sci. Instrum.* **56**:2043, 1985.

[48] Sternin E. Radio frequency phase shifting at the source simplifies NMR spectrometer design. *Rev. Sci. Instrum.* **66**:3144, 1995.

[49] Sternin E., Fine B., Bloom M., Tilcock C., Wong K.F and Cullis P.R. Acyl chain orientational order in the hexagonal H_{II} phase of phospholipid-water dispersions. *Biophys. J.* **54**:689, 1988.

[50] Thewalt J.L., Tullock A.P. and Cushley R.S. A deuterium NMR study of labeled n-alcanol anesthetics in a model membrane. *Chem. Phys. Lipids* **39**:93, 1986.

[51] Thurmond R.L., Niemi A.R., Lindblom G., Wieslander A. and Rilfors L. Membrane thickness and molecular ordering in *Acholeplasma laidlawii* strain A studied by ^{2}H NMR spectroscopy. *Biochemistry* **33**:13178, 1994.

[52] Tikhonov A.N. and Arsenin V.Y. Solutions of III-posed problems. John Wiley, New York, 1977.

[53] Vold R. and Prosser S. Magnetically Oriented Phospholipid Bilayered Micelles for Structural Studies of Polypeptides. Does the Ideal Bicelle Exist? *J. Magn. Reson. B* **113** :267, 1996.

[54] Whittall K., Sternin E., Bloom M. and MacKay A.L. Time and frequency-domain dePakeing using inverse theory. *J. Mag. Res.* **84**:64, 1989.

[55] Yeagle P.L. The Membranes of Cells. Academic Press, INC. 1993.

[56] http://www.uku.fi/perch.html